Abstract

Proton Radiography

Los Alamos National Laboratory has used high energy protons as a probe in flash radiography for a decade. In this time the proton radiography project has used 800 MeV protons, provided by the LANSCE accelerator facility at LANL, to diagnose over three-hundred dynamic experiments in support of national and international weapons science and stockpile stewardship programs. Through this effort significant experience has been gained in using charged particles as direct radiographic probes to diagnose transient systems. The results of this experience will be discussed through the presentation of data from experiments recently performed at the LANL pRad.

Proton Radiography Primer

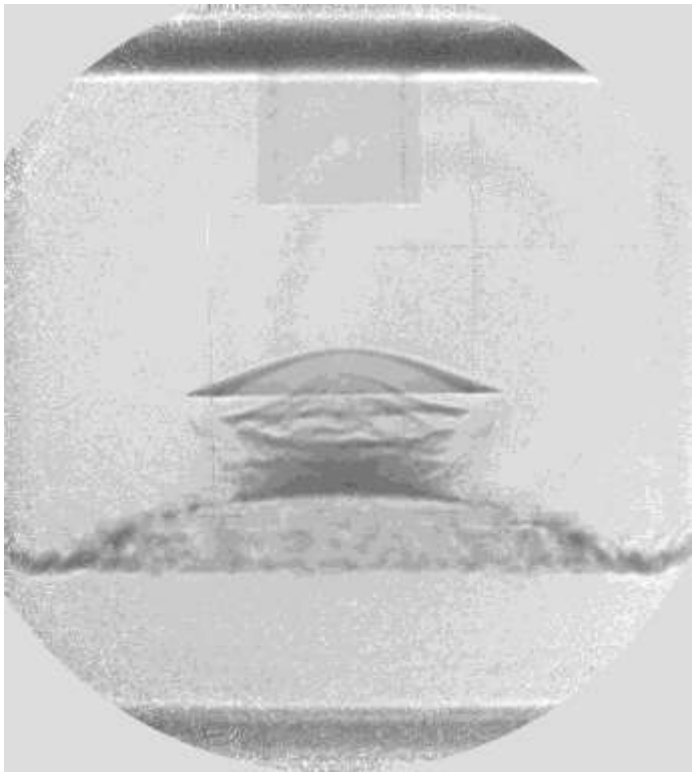

Frank Merrill, LANL
and the pRad collaboration

pRad Collaboration

Bechtel Nevada
Stuart Baker, Alfred Meidinger, Richard Thompson, Josh Tybo
DE-2
Robert Hixson, Paulo Rigg, Darcie Dennis-Kohler
HX-3
Joe Bainbridge, Stephen Dennison, Eric Ferm, Robert Lopez, Mark Marr-Lyon, Carlos Montoya, Paul Rightley Wendy McNeil
LANSCE-1
Andrew Jason, Barbara Blind, Charles Mottershead
LANSCE-6
Leo Bittecker, Rodney McCrady, Chandra Pillai
P-23
William Buttler, David D. Clark, David Holtkamp, Nick King, Kris Kwiatkowski, Kevin Morley, Russ Olson, Paul Nedrow
P-25
Jeffrey Bacon, Bethany Brooks, Camilo Espinoza, Gary Hogan, Brian Hollander, Julian Lopez, Fesseha Mariam, Frank Merrill, Christopher Morris, Matthew Murray, Alexander Saunders, Richard Schirato, Larry Schultz, Cynthia Schwartz, Dale Tupa
S-7
Rodger Liljestrand
X-4
Langdon Bennett, John David Becker, Maria Rightley, Stephen Sterbenz

Proton Interactions

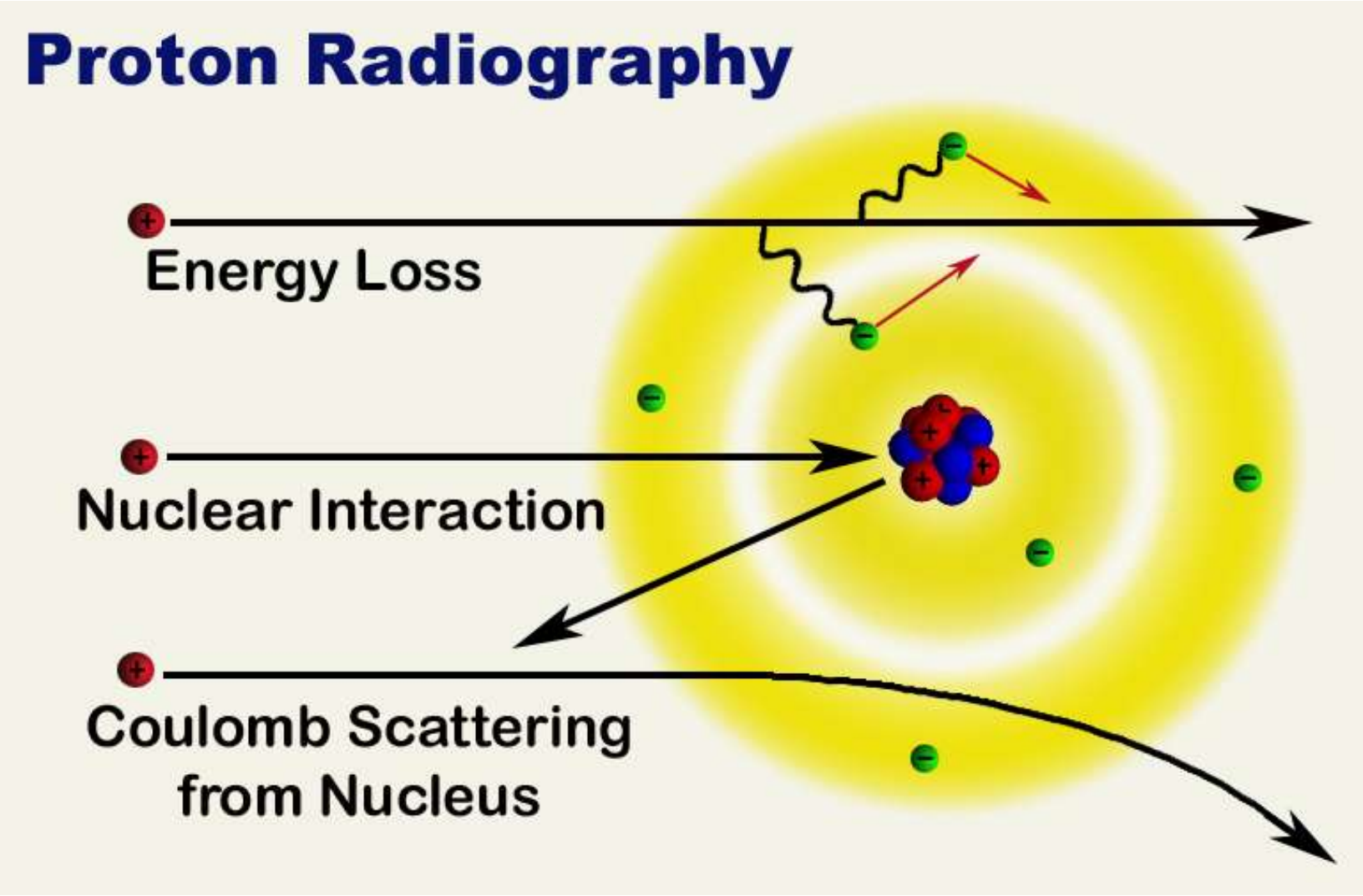

Early Proton Radiography

A. M. Koehler, *et al.* *Science* **160**, 303 (1968)

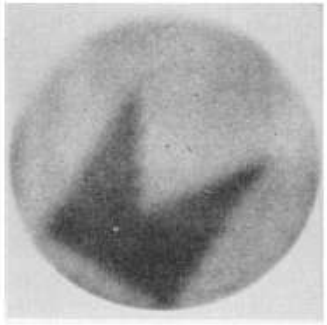

Fig. 1. Proton radiograph of aluminum absorber 7 cm in diameter and 18 g/cm² thick, with an additional thickness of 0.035-g/cm² aluminum foil, cut in the shape of a pennant, inserted at a depth of 9 g/cm². The addition of 0.2 percent to the total thickness produces a substantially darker area on the film.

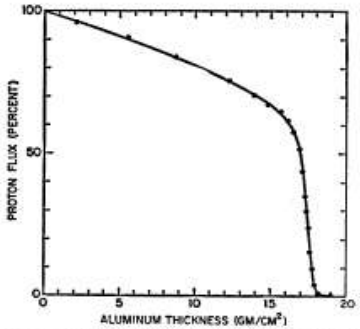

Fig. 2. Proton flux as a function of depth in aluminum. The steeply falling portion of the curve near 18 g/cm² is used to obtain the high contrast of Fig. 1.

J. A. Cookson Naturwissenschaften 61, 184—191 (1974)

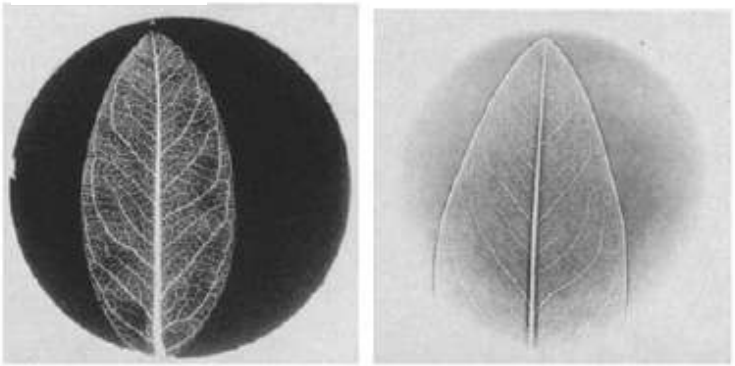

Fig. 6a and b. Radiographs of leaves by a) marginal range radiography with 196 mg/cm² of extra Al absorber, and b) scattering radiography with leaf sandwiched between two 6.9 mg/cm² Al layers and 14 mm from the film

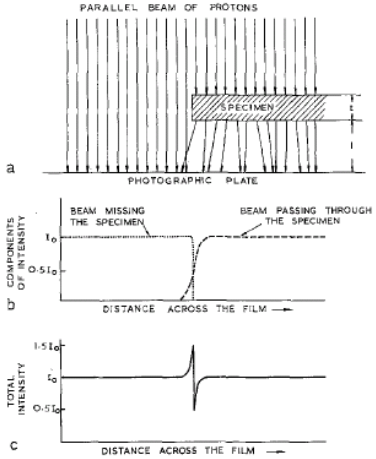

Fig. 7. Illustration of how multiple scattering produces its characteristic edge pattern

Marginal Range Radiography

- Reduce proton beam energy to near end of range.
- Use steep portion of transmission curve to enhance sensitivity to areal density variations.
- Coulomb scattering at low energy results in poor resolution >1.5 mm.
- Contrast generated through proton absorption.

Scattering Radiography

- Edge detection only
- Limited to thin objects
- Contrast generated through position dependent scattering

LANL Transmission Radiography (1995)

188 MeV secondary proton beamline at LANSCE

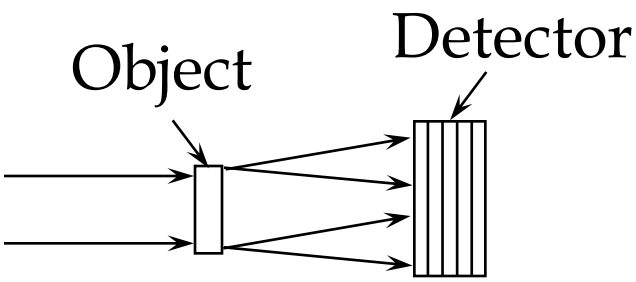

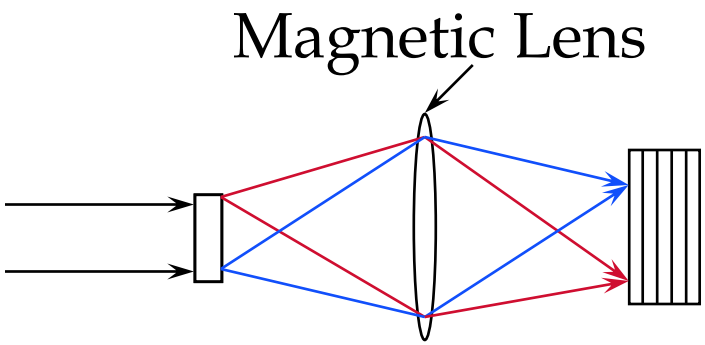

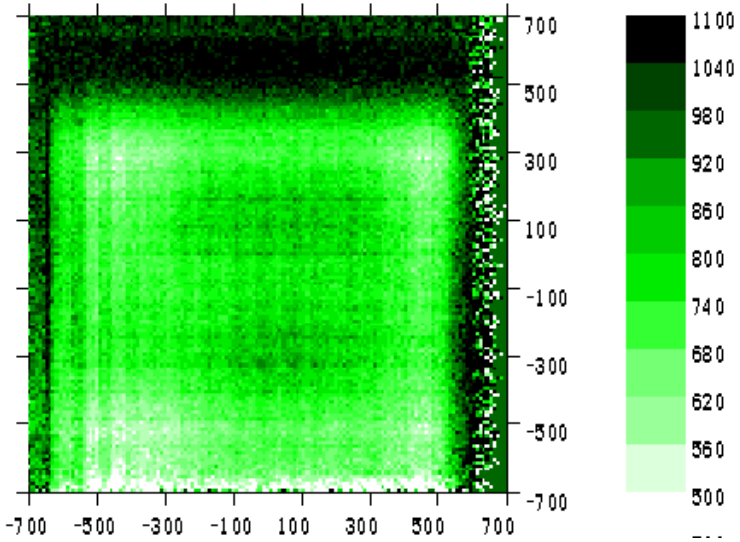

Image at the detector is substantially blurred.

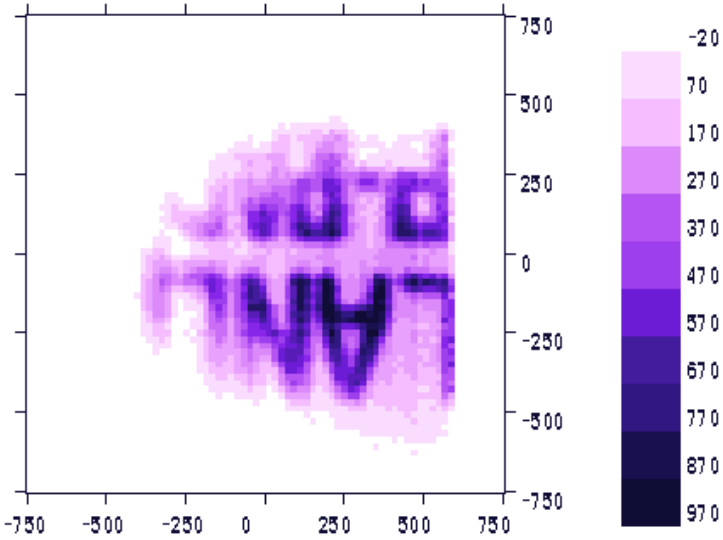

Magnetic imaging lens preserves image with high resolution.

Magnetic Imaging Lens

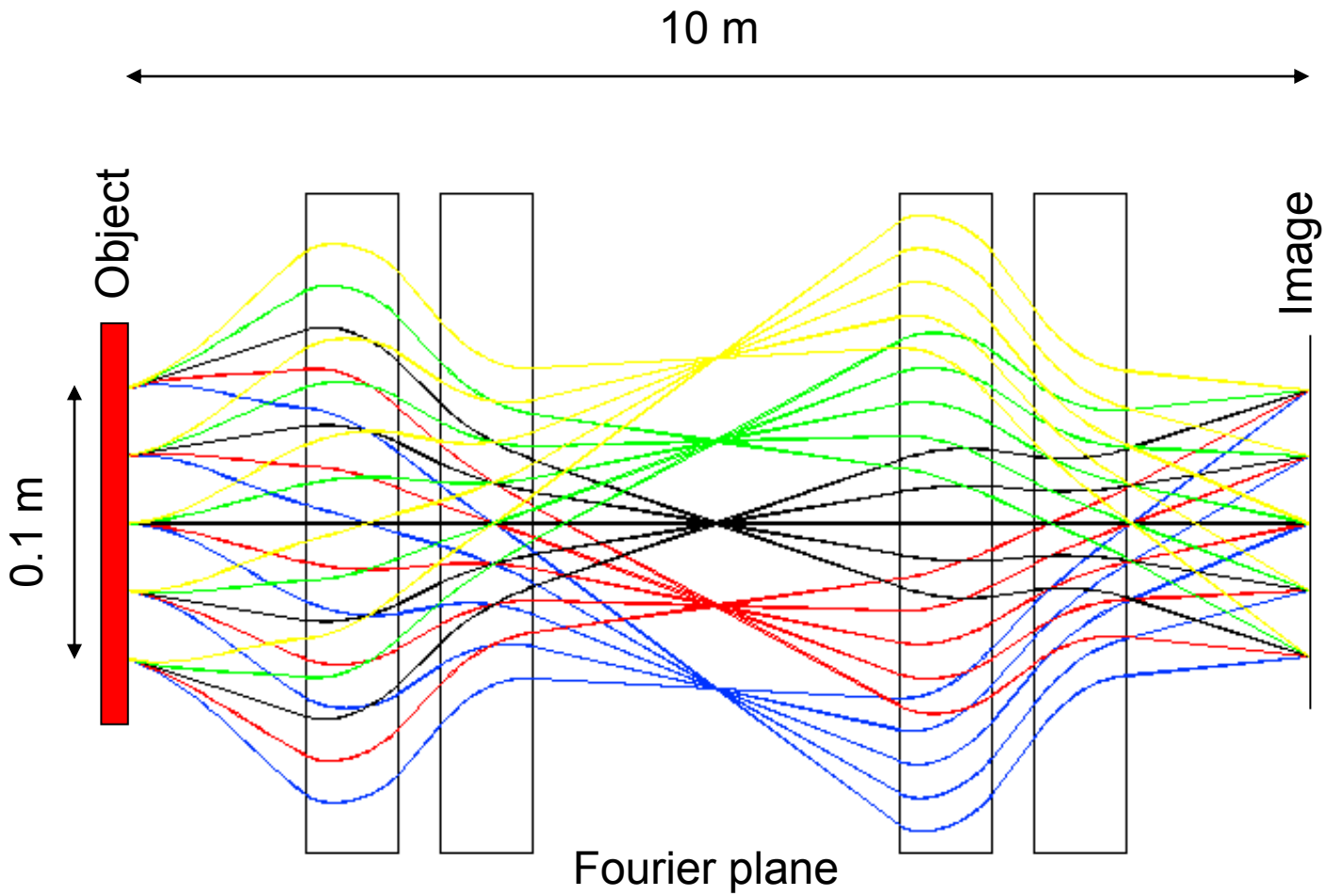

Quadrupole Identity Lens

Multiple Coulomb Scattering

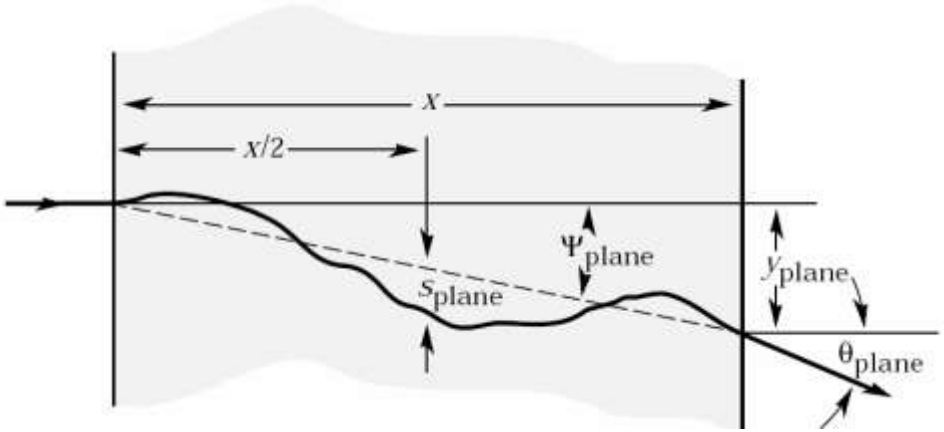

$$\theta_o = \frac{13.6MeV}{\beta p}\sqrt{x/X_o}\left[1+0.038\ln\left(x/X_o\right)\right]$$ *

RMS Width

Full Width Half Maximum=2.35 θ_o

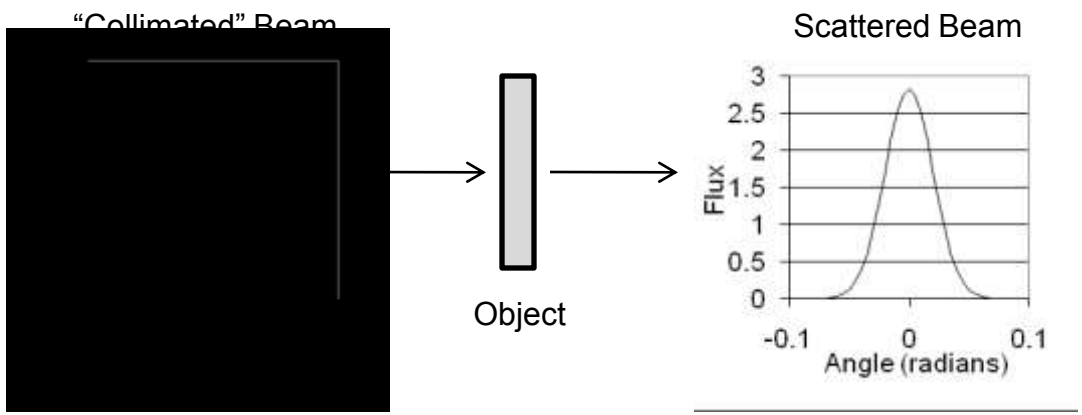

$$\theta_o = \frac{14.1MeV}{\beta p}\sqrt{x/X_o}$$

Typical LANL simplification

*C. Amsler et al., Physics Letters **B667**, 1 (2008)

Contrast from Multiple Coulomb Scattering

Incident Beam

After Object

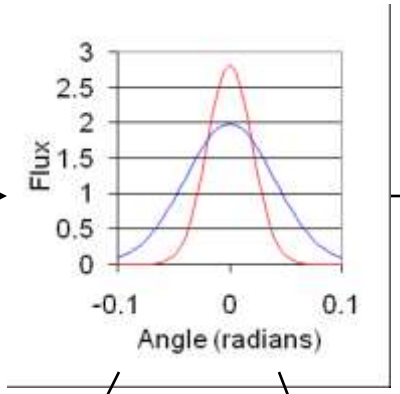

After Collimator

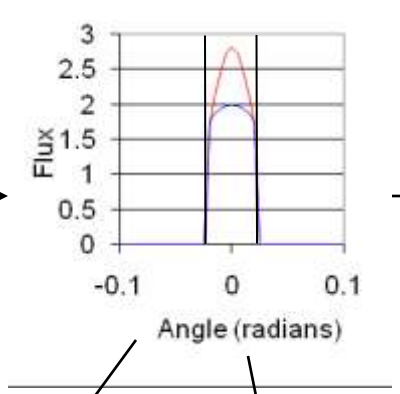

Measured transmission provides information of object thickness

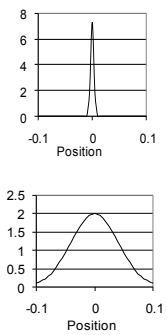

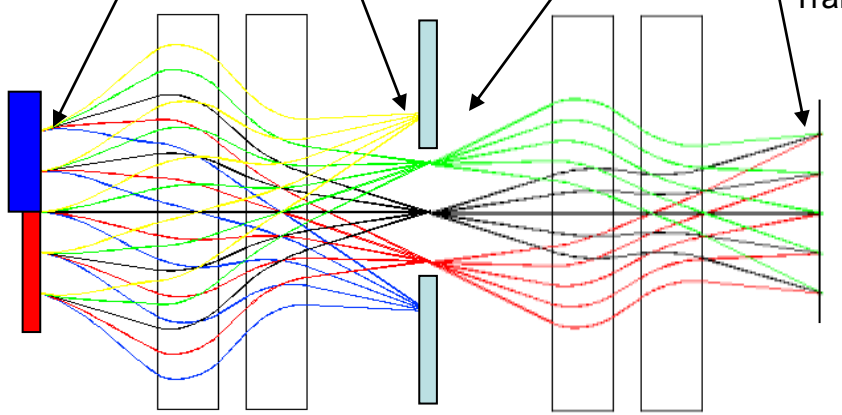

Collimator

Transmission

Transmission

$$T_{MCS} = 1 - e^{-\theta_c^2 / 2\theta_o^2}$$

Nuclear Interactions

Angular distribution of 800 MeV proton nuclear elastic scattering from Iron.

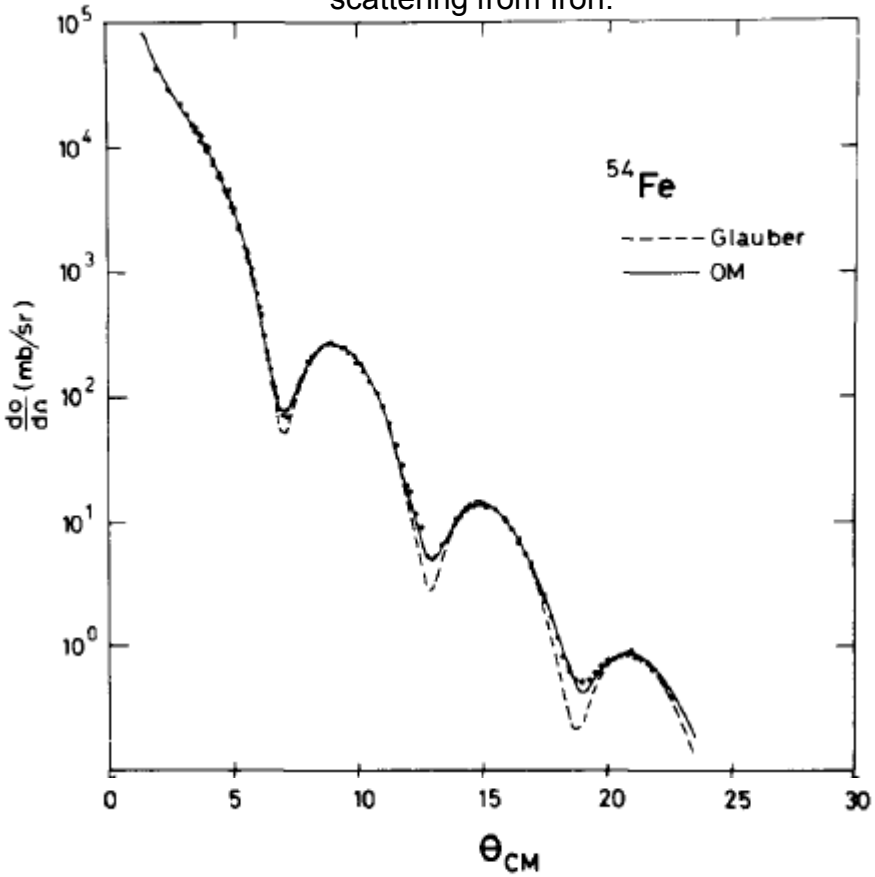

Simple Approximation for Modeling Proton Radiography

- Characteristic Nuclear Collision Length: λ_c
- Approximate that each interaction removes the proton from the acceptance of the imaging lens.
- Measure the collision Length at 800 MeV

The "true" nuclear interactions are more complicated than this simple assumption and these interactions are reasonably well understood. This can all be simulated, but it is typically not worth the effort for designing small scale experiments.

Transmission

$$T_{nuclear} = e^{-x/\lambda_c}$$

Transmission Calculation

$$T_{nuclear} = e^{-x/\lambda_c}$$

Nuclear removal processes:

☺$_o$ - scattering angle (radians)

x - areal density

$$T_{MCS} = 1 - e^{-\theta_c^2 / 2\theta_o^2}$$

$$\theta_o = \frac{14.1MeV}{p\beta}\sqrt{\frac{x}{x_o}}$$

Multiple Coulomb Scattering with collimation:

☺$_o$ - scattering angle (radians)

x - areal density

x_o - radiation length

p - momentum (MeV)

β - relativistic velocity

$$T = e^{-x/\lambda_c}\left(1 - e^{-\left(\frac{\theta_c p\beta}{14.1MeV}\right)^2 \frac{x_o}{2x}}\right)$$

Total EstimatedTransmission:

Good to 5-10%

Particle Data Group:
http://pdg.lbl.gov/

A Useful Table

6. ATOMIC AND NUCLEAR PROPERTIES OF MATERIALS

Table 6.1 Abridged from `pdg.lbl.gov/AtomicNuclearProperties` by D. E. Groom (2007). See web pages for more detail about entries in this table including chemical formulae, and for several hundred other entries. Quantities in parentheses are for NTP (20° C and 1 atm), and square brackets indicate quantities evaluated at STP. Boiling points are at 1 atm. Refractive indices n are evaluated at the sodium D line blend (589.2 nm); values $\gg 1$ in brackets are for $(n-1)\times 10^6$ (gases).

Material	Z	A	$\langle Z/A \rangle$	Nucl.coll. length λ_T {g cm^{-2}}	Nucl.inter. length λ_I {g cm^{-2}}	Rad.len. X_0 {g cm^{-2}}	$dE/dx\|_{\rm min}$ { MeV g^{-1}cm^2}	Density {g cm^{-3}} ({gℓ^{-1}})	Melting point (K)	Boiling point (K)	Refract. index (@ Na D)
H_2	1	1.00794(7)	0.99212	42.8	52.0	63.04	(4.103)	0.071(0.084)	13.81	20.28	1.11[132.]
D_2	1	2.01410177803(8)	0.49650	51.3	71.8	125.97	(2.053)	0.169(0.168)	18.7	23.65	1.11[138.]
He	2	4.002602(2)	0.49967	51.8	71.0	94.32	(1.937)	0.125(0.166)		4.220	1.02[35.0]
Li	3	6.941(2)	0.43221	52.2	71.3	82.78	1.639	0.534	453.6	1615.	
Be	4	9.012182(3)	0.44384	55.3	77.8	65.19	1.595	1.848	1560.	2744.	
C diamond	6	12.0107(8)	0.49955	59.2	85.8	42.70	1.725	3.520			2.42
C graphite	6	12.0107(8)	0.49955	59.2	85.8	42.70	1.742	2.210			
N_2	7	14.0067(2)	0.49976	61.1	89.7	37.99	(1.825)	0.807(1.165)	63.15	77.29	1.20[298.]
O_2	8	15.9994(3)	0.50002	61.3	90.2	34.24	(1.801)	1.141(1.332)	54.36	90.20	1.22[271.]
F_2	9	18.9984032(5)	0.47372	65.0	97.4	32.93	(1.676)	1.507(1.580)	53.53	85.03	[195.]
Ne	10	20.1797(6)	0.49555	65.7	99.0	28.93	(1.724)	1.204(0.839)	24.56	27.07	1.09[67.1]
Al	13	26.9815386(8)	0.48181	69.7	107.2	24.01	1.615	2.699	933.5	2792.	
Si	14	28.0855(3)	0.49848	70.2	108.4	21.82	1.664	2.329	1687.	3538.	3.95
Cl_2	17	35.453(2)	0.47951	73.8	115.7	19.28	(1.630)	1.574(2.980)	171.6	239.1	[773.]
Ar	18	39.948(1)	0.45059	75.7	119.7	19.55	(1.519)	1.396(1.662)	83.81	87.26	1.23[281.]
Ti	22	47.867(1)	0.45961	78.8	126.2	16.16	1.477	4.540	1941.	3560.	
Fe	26	55.845(2)	0.46557	81.7	132.1	13.84	1.451	7.874	1811.	3134.	
Cu	29	63.546(3)	0.45636	84.2	137.3	12.86	1.403	8.960	1358.	2835.	
Ge	32	72.64(1)	0.44053	86.9	143.0	12.25	1.370	5.323	1211.	3106.	
Sn	50	118.710(7)	0.42119	98.2	166.7	8.82	1.263	7.310	505.1	2875.	
Xe	54	131.293(6)	0.41129	100.8	172.1	8.48	(1.255)	2.953(5.483)	161.4	165.1	1.39[701.]
W	74	183.84(1)	0.40252	110.4	191.9	6.76	1.145	19.300	3695.	5828.	
Pt	78	195.084(9)	0.39983	112.2	195.7	6.54	1.128	21.450	2042.	4098.	
Au	79	196.966569(4)	0.40108	112.5	196.3	6.46	1.134	19.320	1337.	3129.	
Pb	82	207.2(1)	0.39575	114.1	199.6	6.37	1.122	11.350	600.6	2022.	
U	92	[238.02891(3)]	0.38651	118.6	209.0	6.00	1.081	18.950	1408.	4404.	
Air (dry, 1 atm)			0.49919	61.3	90.1	36.62	(1.815)	(1.205)		78.80	
Shielding concrete			0.50274	65.1	97.5	26.57	1.711	2.300			
Borosilicate glass (Pyrex)			0.49707	64.6	96.5	28.17	1.696	2.230			
Lead glass			0.42101	95.9	158.0	7.87	1.255	6.220			
Standard rock			0.50000	66.8	101.3	26.54	1.688	2.650			
Methane (CH_4)			0.62334	54.0	73.8	46.47	(2.417)	(0.667)	90.68	111.7	[444.]
Ethane (C_2H_6)			0.59861	55.0	75.9	45.66	(2.304)	(1.263)	90.36	184.5	
Propane (C_3H_8)			0.58962	55.3	76.7	45.37	(2.262)	0.493(1.868)	85.52	231.0	
Butane (C_4H_{10})			0.59497	55.5	77.1	45.23	(2.278)	(2.489)	134.9	272.6	
Octane (C_8H_{18})			0.57778	55.8	77.8	45.00	2.123	0.703	214.4	398.8	
Paraffin ($CH_3(CH_2)_{n\approx 23}CH_3$)			0.57275	56.0	78.3	44.85	2.088	0.930			
Nylon (type 6, 6/6)			0.54790	57.5	81.6	41.92	1.973	1.18			
Polycarbonate (Lexan)			0.52697	58.3	83.6	41.50	1.886	1.20			
Polyethylene ($[CH_2CH_2]_n$)			0.57034	56.1	78.5	44.77	2.079	0.89			
Polyethylene terephthalate (Mylar)			0.52037	58.9	84.9	39.95	1.848	1.40			
Polyimide film (Kapton)			0.51264	59.2	85.5	40.58	1.820	1.42			
Polymethylmethacrylate (acrylic)			0.53937	58.1	82.8	40.55	1.929	1.19			1.49
Polypropylene			0.55998	56.1	78.5	44.77	2.041	0.90			
Polystyrene ($[C_6H_5CHCH_2]_n$)			0.53768	57.5	81.7	43.79	1.936	1.06			1.59
Polytetrafluoroethylene (Teflon)			0.47992	63.5	94.4	34.84	1.671	2.20			
Polyvinyltoluene			0.54141	57.3	81.3	43.90	1.956	1.03			1.58
Aluminum oxide (sapphire)			0.49038	65.5	98.4	27.94	1.647	3.970	2327.	3273.	1.77
Barium flouride (BaF_2)			0.42207	90.8	149.0	9.91	1.303	4.893	1641.	2533.	1.47
Bismuth germanate (BGO)			0.42065	96.2	159.1	7.97	1.251	7.130	1317.		2.15
Carbon dioxide gas (CO_2)			0.49989	60.7	88.9	36.20	1.819	(1.842)			[449.]
Solid carbon dioxide (dry ice)			0.49989	60.7	88.9	36.20	1.787	1.563	Sublimes at 194.7 K		
Cesium iodide (CsI)			0.41569	100.6	171.5	8.39	1.243	4.510	894.2	1553.	1.79
Lithium fluoride (LiF)			0.46262	61.0	88.7	39.26	1.614	2.635	1121.	1946.	1.39
Lithium hydride (LiH)			0.50321	50.8	68.1	79.62	1.897	0.820	965.		
Lead tungstate ($PbWO_4$)			0.41315	100.6	168.3	7.39	1.229	8.300	1403.		2.20
Silicon dioxide (SiO_2, fused quartz)			0.49930	65.2	97.8	27.05	1.699	2.200	1986.	3223.	1.46
Sodium chloride (NaCl)			0.55509	71.2	110.1	21.91	1.847	2.170	1075.	1738.	1.54
Sodium iodide (NaI)			0.42697	93.1	154.6	9.49	1.305	3.667	933.2	1577.	1.77
Water (H_2O)			0.55509	58.5	83.3	36.08	1.992	1.000(0.756)	273.1	373.1	1.33
Silica aerogel			0.50093	65.0	97.3	27.25	1.740	0.200	(0.03 H_2O, 0.97 SiO_2)		

Accurate Areal Density Reconstructions

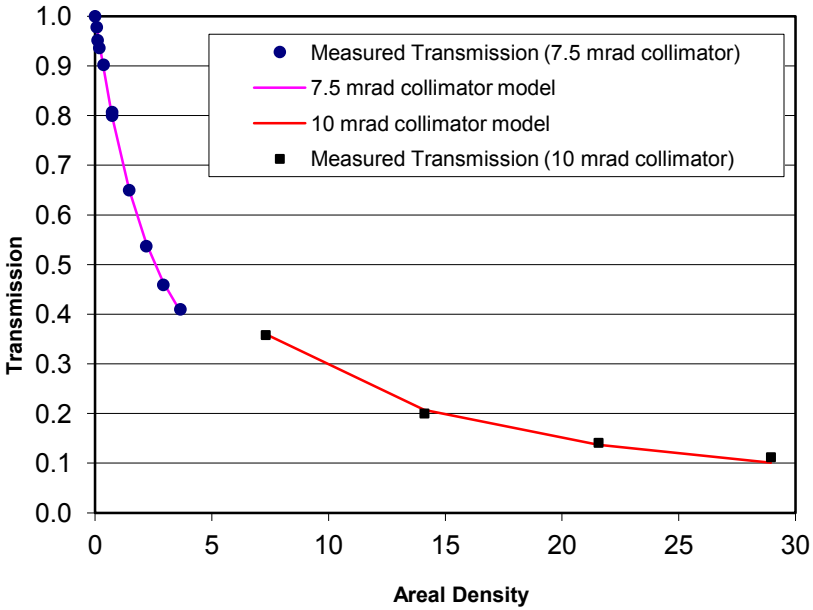

Build a step wedge and adjust parameters to fit measured data

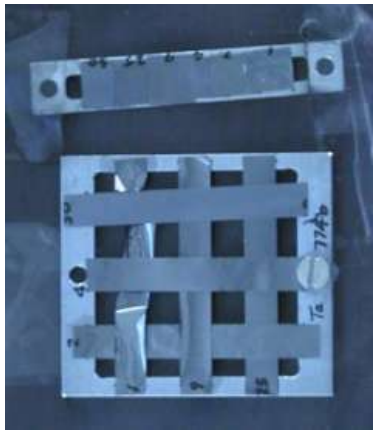

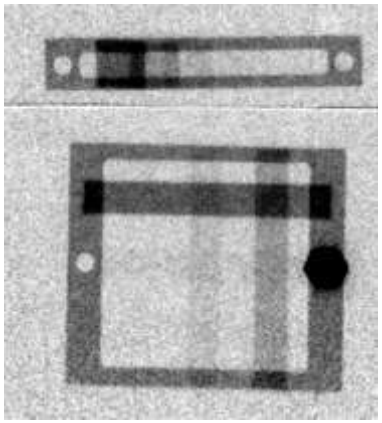

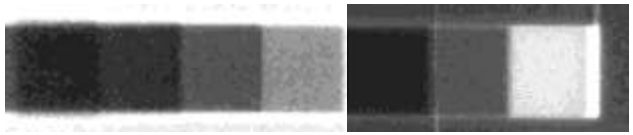

$$T = e^{-\left(x/\lambda_c + \left(\frac{\theta_c p \beta}{14.1 MeV}\right)^2 \frac{x_o}{2(x+x_f)} \right)}$$

Adjust parameters to fit transmission data:

- λ_c - nuclear collision length
- X_f – fixed radiation length (windows, beam angular spread)

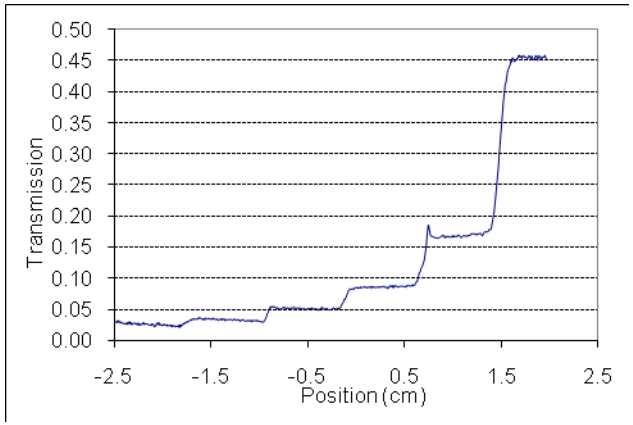

When is an object too thick?

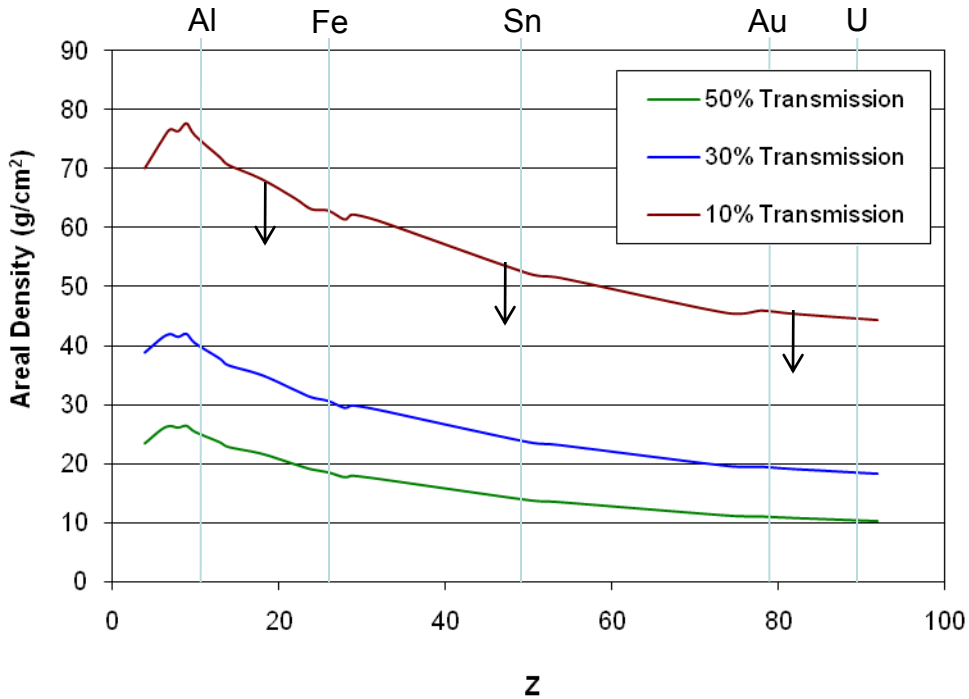

Areal density contours of constant transmission as a function of atomic number.

10% is near the lower limit of reasonable transmission.

Dynamic Range of 800 MeV Proton Radigraphy

$$FOM = \frac{\Delta N / \sqrt{N}}{\Delta l / l} = \frac{l}{\sqrt{T}} \frac{dT}{dl}$$

Signal to noise

Fractional change in thickness

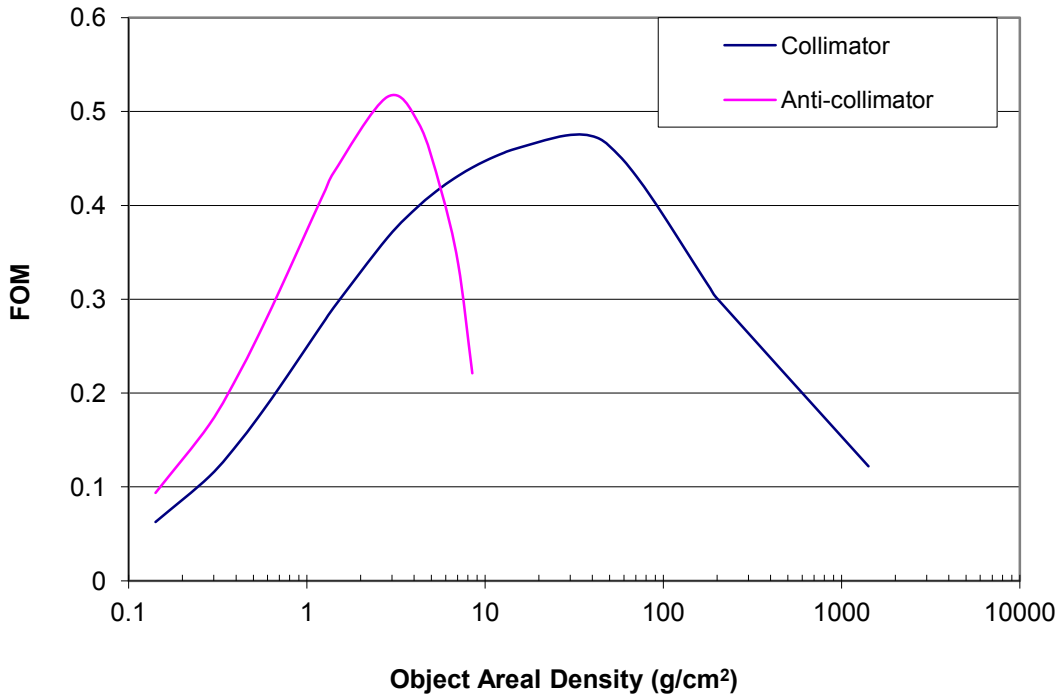

- 800 MeV proton radiography ranges from 1 g/cm^2 up to 70 g/cm^2 of iron

LANSCE Experimental Areas

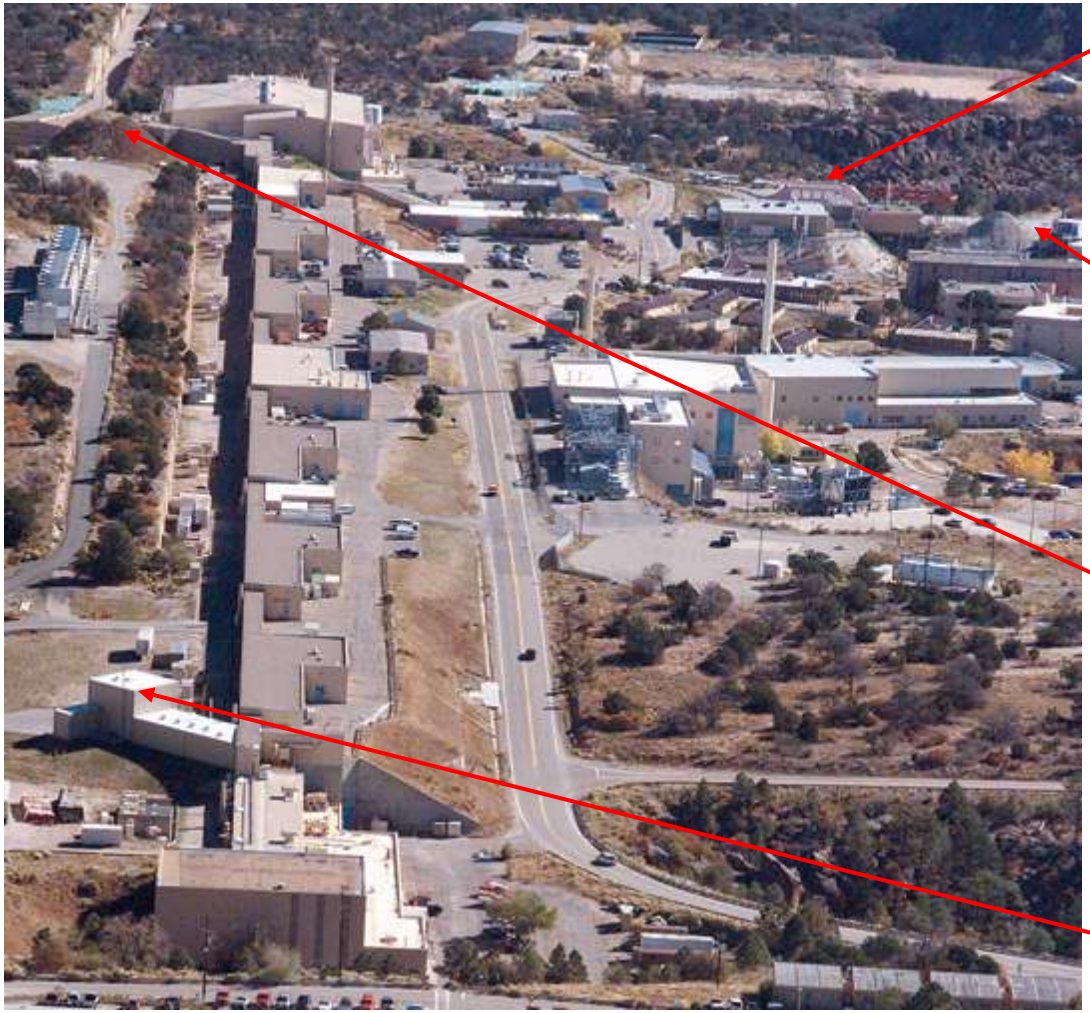

- Lujan Center
  - ***National security research***
  - ***Materials, bio-science, and nuclear physics***
  - ***National user facility***
- WNR
  - ***National security research***
  - ***Nuclear Physics***
  - ***Neutron Irradiation***
- Proton Radiography
  - ***National security research***
  - ***Dynamic Materials science,***
  - ***Hydrodynamics***
- Isotope Production Facility
  - ***Medical radioisotopes***

Full LANSCE System

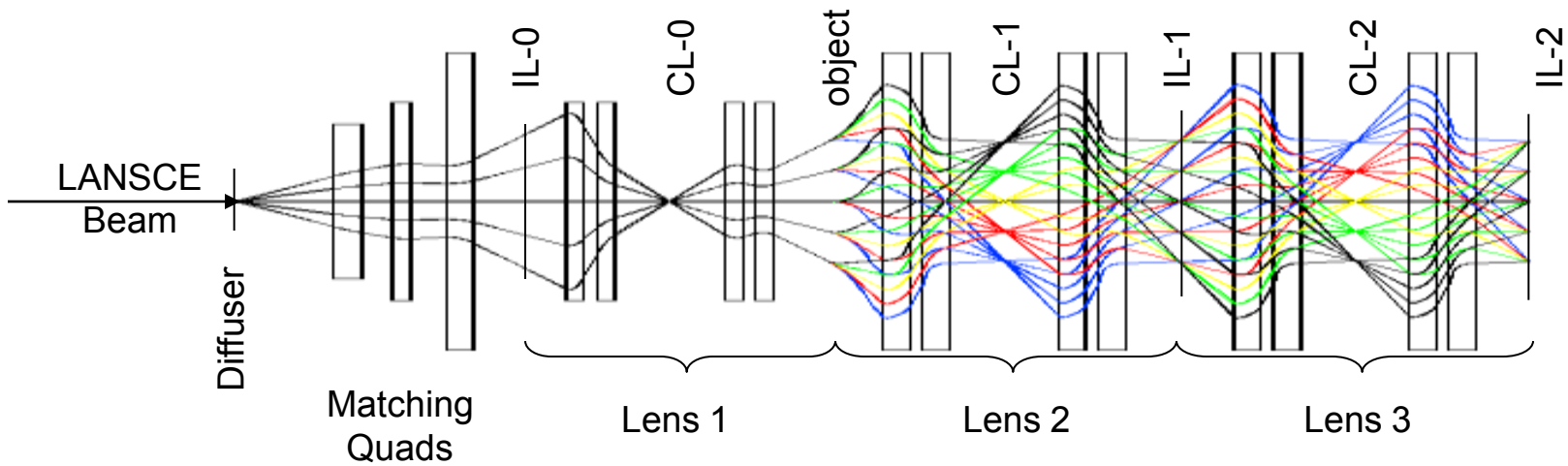

- Diffuser sets illumination pattern at object.
- Matching quads establish position-angle correlation
- CL-0 has a 9.0 mRad collimator
- CL-1 and CL-2 can independently have 5-20 mrad collimators
- Lens 0 used for beam monitoring
- IL-1 has seven single-shot camera systems
- IL-2 has five single-shot camera systems and a 9-frame framing camera
- 21 images per dynamic event at up to 21 different times.

800 MeV pRad Facility at LANSCE

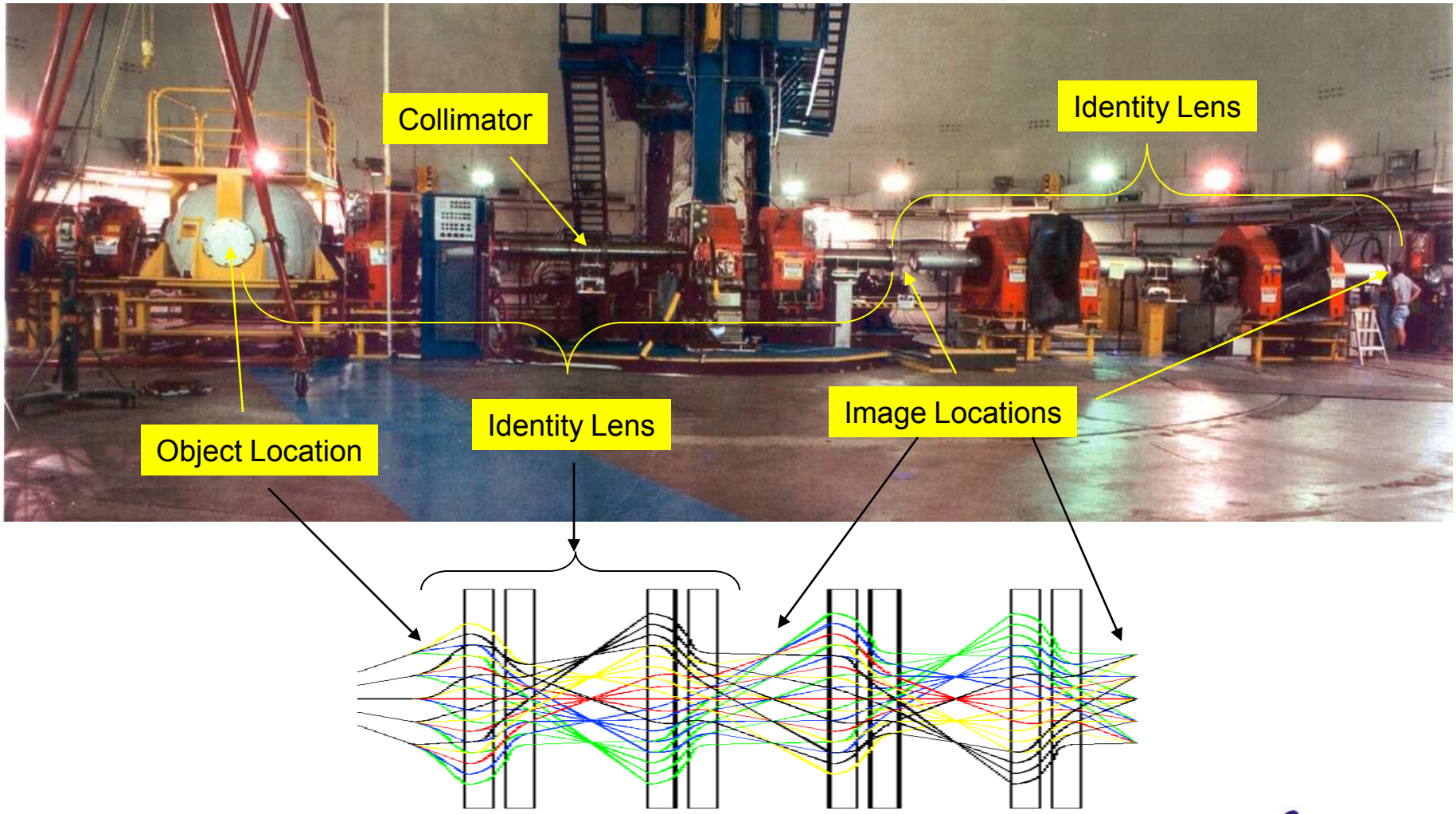

Temporal Resolution

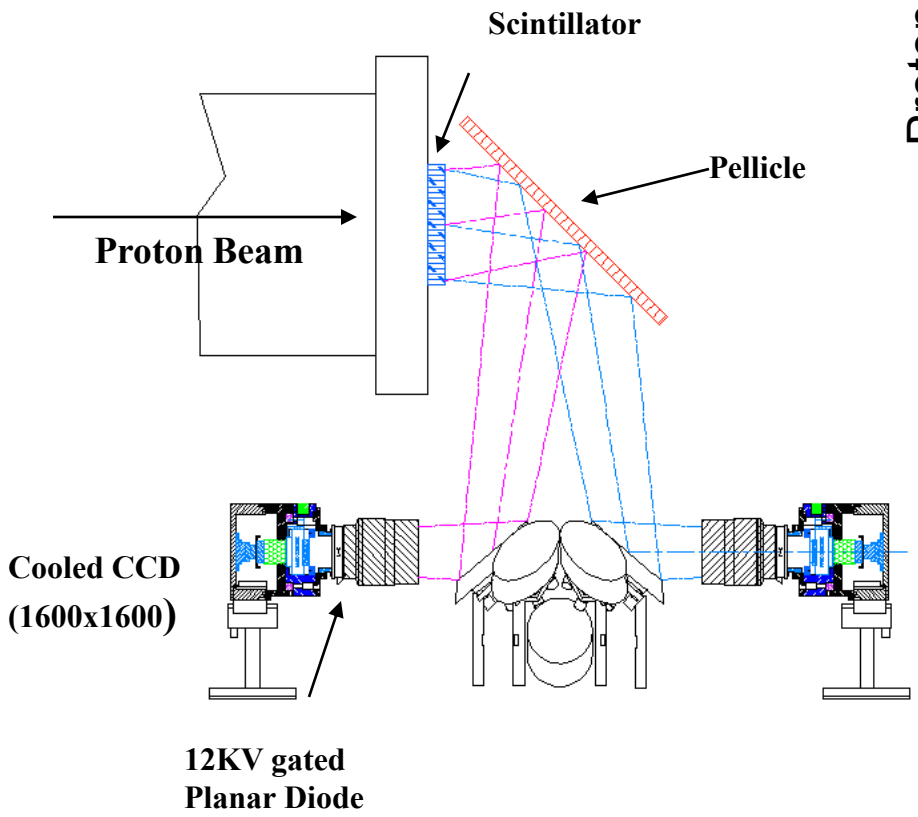

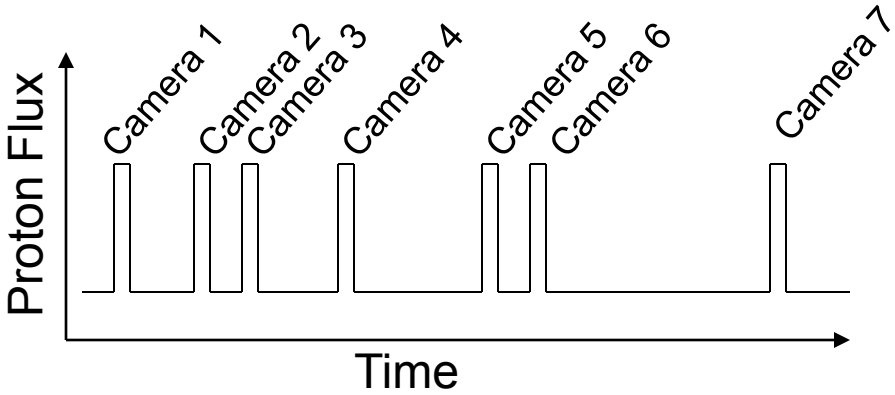

- 19 images at first station
- 22 images at second station
- Typically 100 ns exposure times

Chromatic Aberration and Resolution

Identity Lens

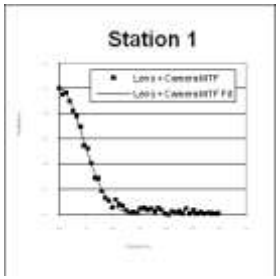

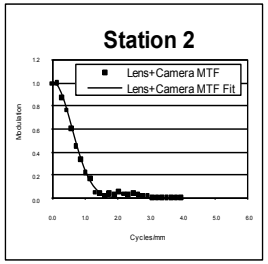

- 12 inch lens
- Station 1: 178 μm
- Station 2: 280 μm
- Gaussian blur function.
- 120 mm field of view

X3 Magnifier

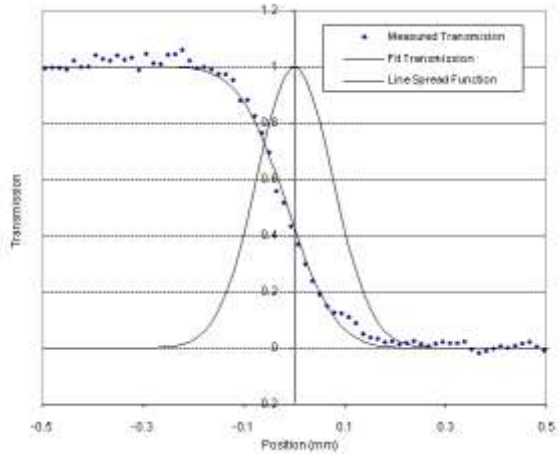

2.5 lp/mm

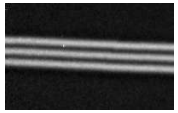

- 4 inch lens
- Station 1: 65 μm
- Gaussian blur function.
- 44 mm field of view

X7 Lens

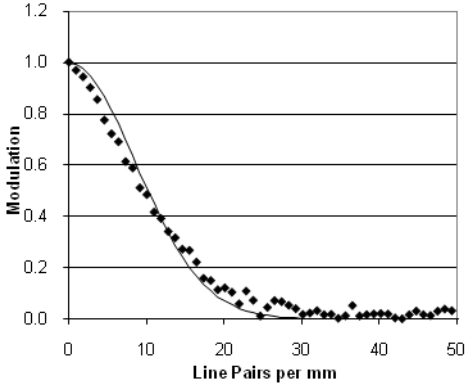

- 1 inch lens
- Station 1: 30 μm
- Gaussian blur function.
- 17 mm field of view

Radiographic Analysis

"Raw" Radiograph

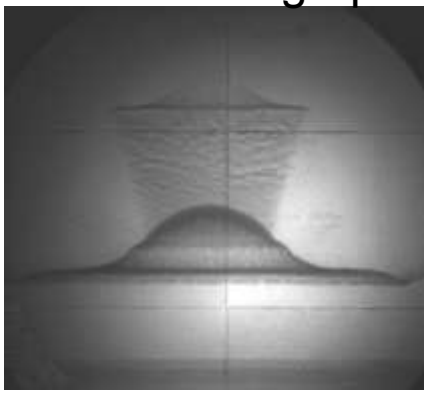

-

Dark Field

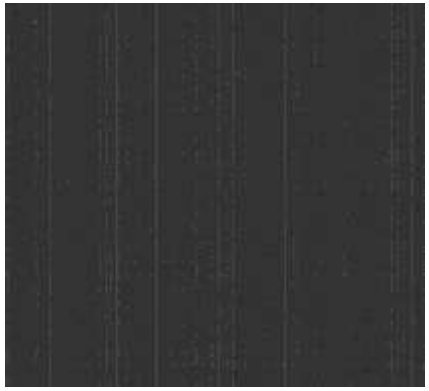

=

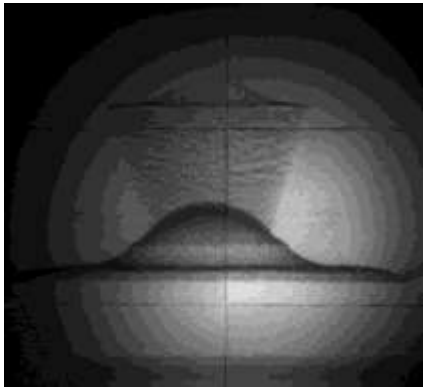

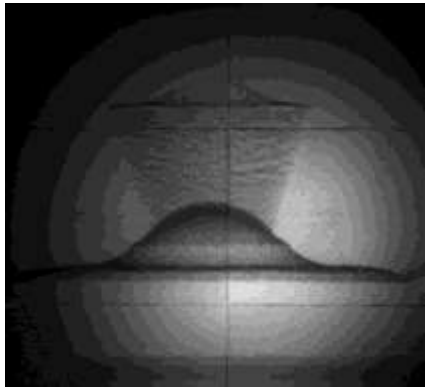

÷

Beam Picture

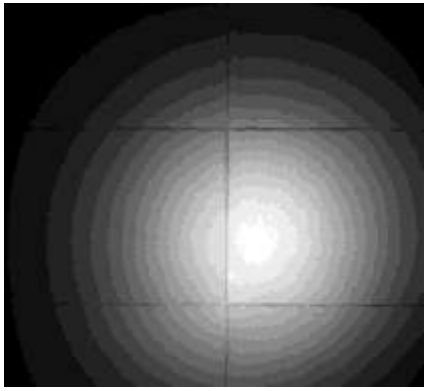

=

Transmission

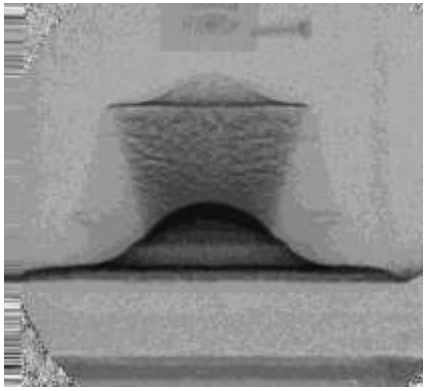

Bethe-Bloch Energy Loss for 800 MeV Protons

$$-\frac{dE}{dx} = Kz^2 \frac{Z}{A} \frac{1}{\beta^2} \left[\frac{1}{2} \ln \frac{2m_e c^2 \beta^2 \gamma^2 T_{\max}}{I^2} - \beta^2 \right] \approx 1.5 \frac{MeV}{g/cm^2}$$

$$K = 4\pi N_A r_e^2 m_e c^2 = 0.307 \frac{MeV}{g/cm^2}$$

$$T_{\max} = \frac{2m_e c^2 \beta^2 \gamma^2}{1 + 2\gamma m_e/M + (m_e/M)^2}$$

C. Amsler et al., Physics Letters **B667**, 1 (2008)

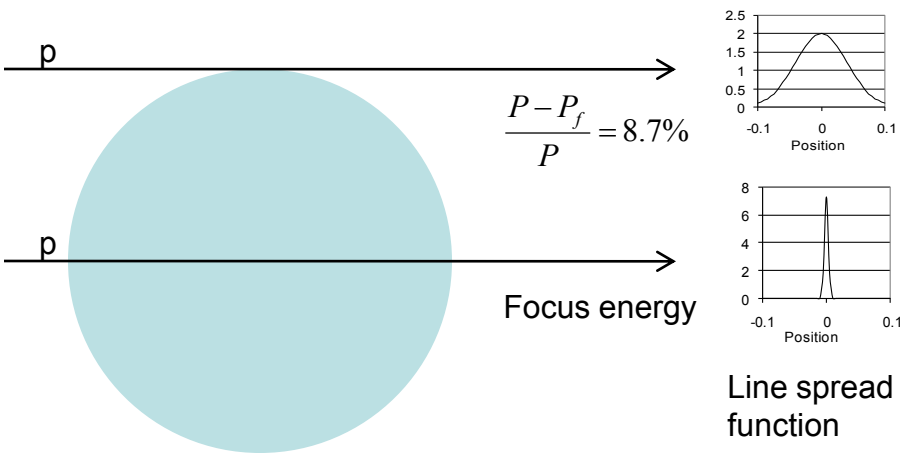

Line spread function

Identity Lens $\frac{P-P_f}{P} = 8.7\%$

copper

Density Reconstruction

Invert to calculate Areal Density

$$T = e^{-x/\lambda}\left(1 - e^{-\left(\frac{\theta_c p\beta}{14.1MeV}\right)^2 \frac{x_o}{2x}}\right)$$

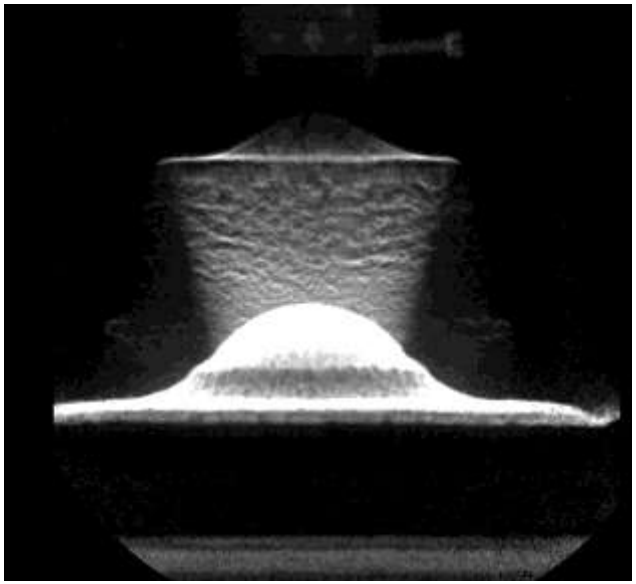

Areal Density (g/cm^2)

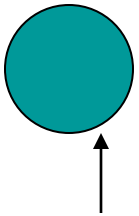

Use assumption of cylindrical symmetry to determine volume density (Abel inversion)

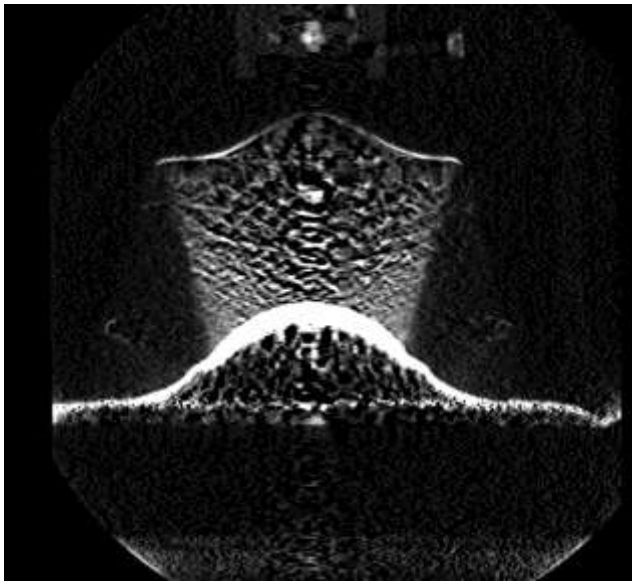

Volume Density (g/cm^3)

Multi-Frame Radiographic Movies

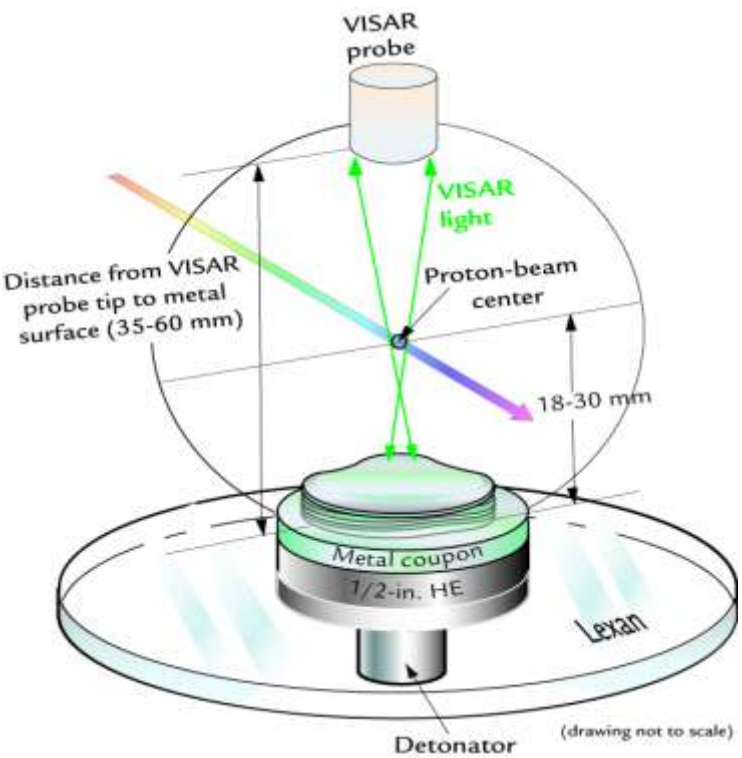

Resolution of Proton Radiography

1. **Object scattering** - introduced as the protons are scattered while traversing the object.
2. **Chromatic aberrations**- introduced as the protons pass through the magnetic lens imaging system.
3. **Detector blur**- introduced as the proton interacts with the proton-to-light converter and as the light is gated and collected with a camera system.

Assume detector development can keep up

Object Scattering

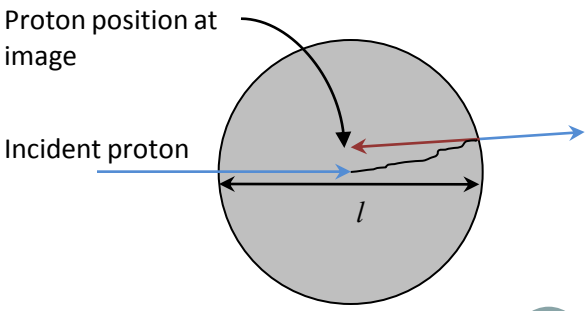

$$\sigma_o = \frac{1}{\sqrt{3}}\theta\frac{l}{2} = \frac{14.1}{\sqrt{6}}\frac{1}{P\beta}\sqrt{\frac{l^3}{x_o}} \propto \frac{l^{3/2}}{P}$$

Chromatic Aberrations

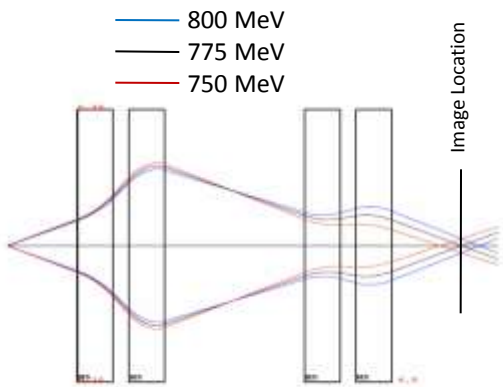

$$\sigma_c = l_c\theta\frac{\delta P}{P^2}\frac{14.1}{\beta}\sqrt{\frac{l}{x_o}} \propto \sqrt{\frac{l}{P^3}}$$

Detector Blur

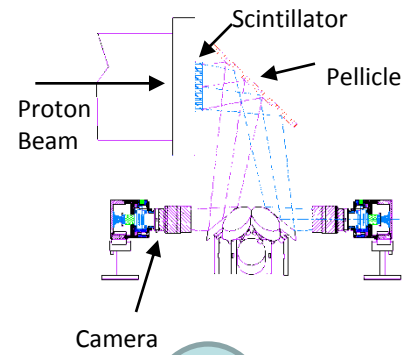

Scintillator

Camera

$$\sigma_s = \theta l_s \propto \frac{l_s\sqrt{l}}{P}$$

Resolution is independent of proton energy

Measurements of Object Scattering Blur

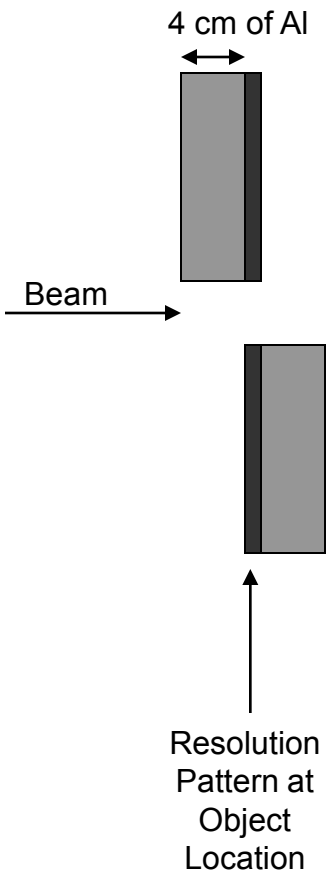

2.5 lp/mm

Sigma=0.061 mm

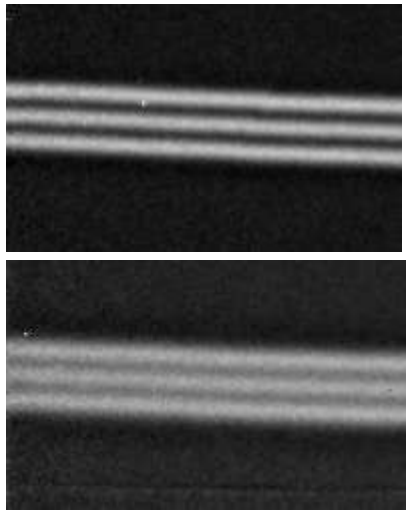

Sigma=0.150 mm

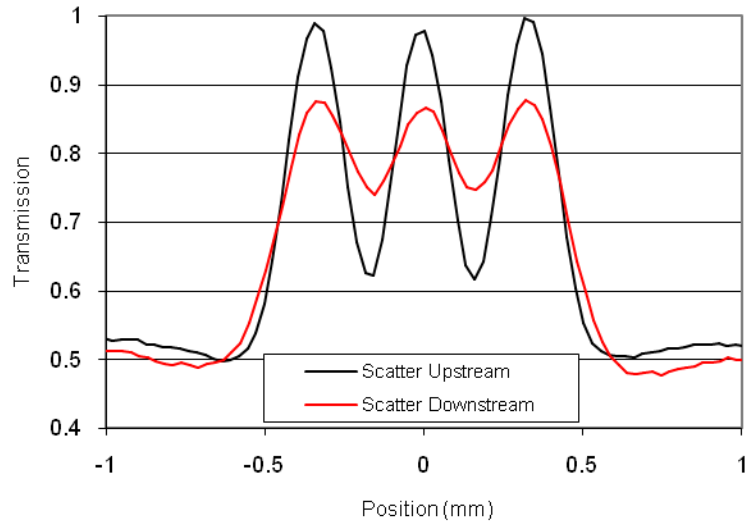

$$\sigma_o = \frac{1}{\sqrt{3}}\theta\frac{l}{2} = \frac{14.1}{\sqrt{6}}\frac{1}{P\beta}\sqrt{\frac{l^3}{x_o}} \propto \frac{l^{3/2}}{P}$$

Correcting Second Order Chromatic Aberrations

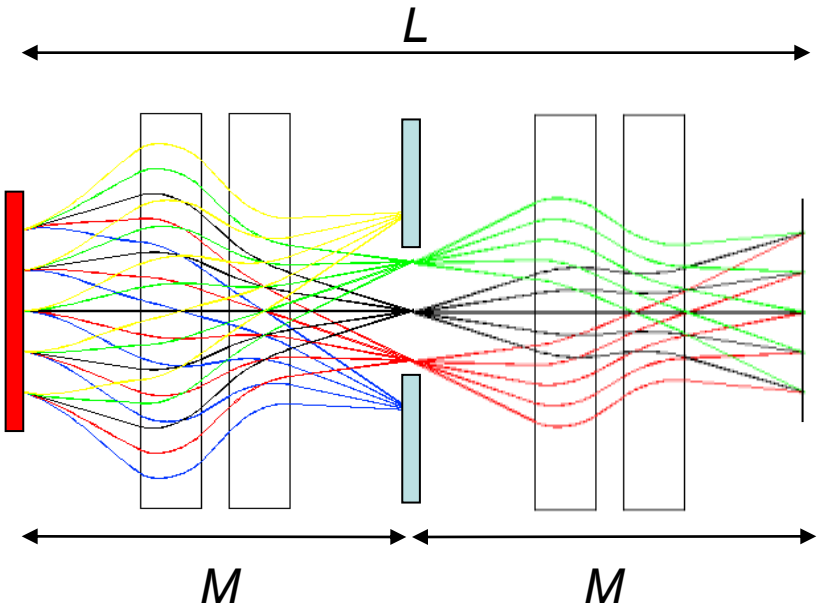

x_o, x_o' - position and angle at object
x_{fp} - position at midpoint of lens
x_i - position and angle at image
δ - $\Delta p/p$
M - Transport matrix for doublet
L - First order Transport matrix
T - Second order Transport tensor

$$L = M^2 = -I$$

Form identity lens from identical doublets

Resolution

$$x_i = L_{11}x_o + L_{12}x_o' + T_{116}x_o\delta + T_{126}x_o'\delta$$

$$x_i = -x_o + T_{116}x_o\delta + T_{126}(wx_o + \phi)\delta$$

$$w = {-T_{116}}/{T_{126}} = {-M_{11}}/{M_{12}}$$

$$w = {-M_{11}}/{M_{12}}$$

$$\Delta x_i = T_{126}\phi\delta$$

Dominates Blur

Inject beam with position-angle correlation to form Fourier plane at center of lens.

Fourier Plane

$$x_{fp} = M_{11}x_o + M_{12}x_o'$$

$$x_o' = wx_o + \phi$$

$$x_{fp} = M_{11}x_o + M_{12}\left(wx_o + \phi\right)$$

$$w = {-M_{11}}/{M_{12}}$$

$$x_{fp} = M_{12}\phi$$

Same position-angle correlation which forms a Fourier plane at the center of the lens also cancels second order chromatic terms.

Chromatic Aberrations

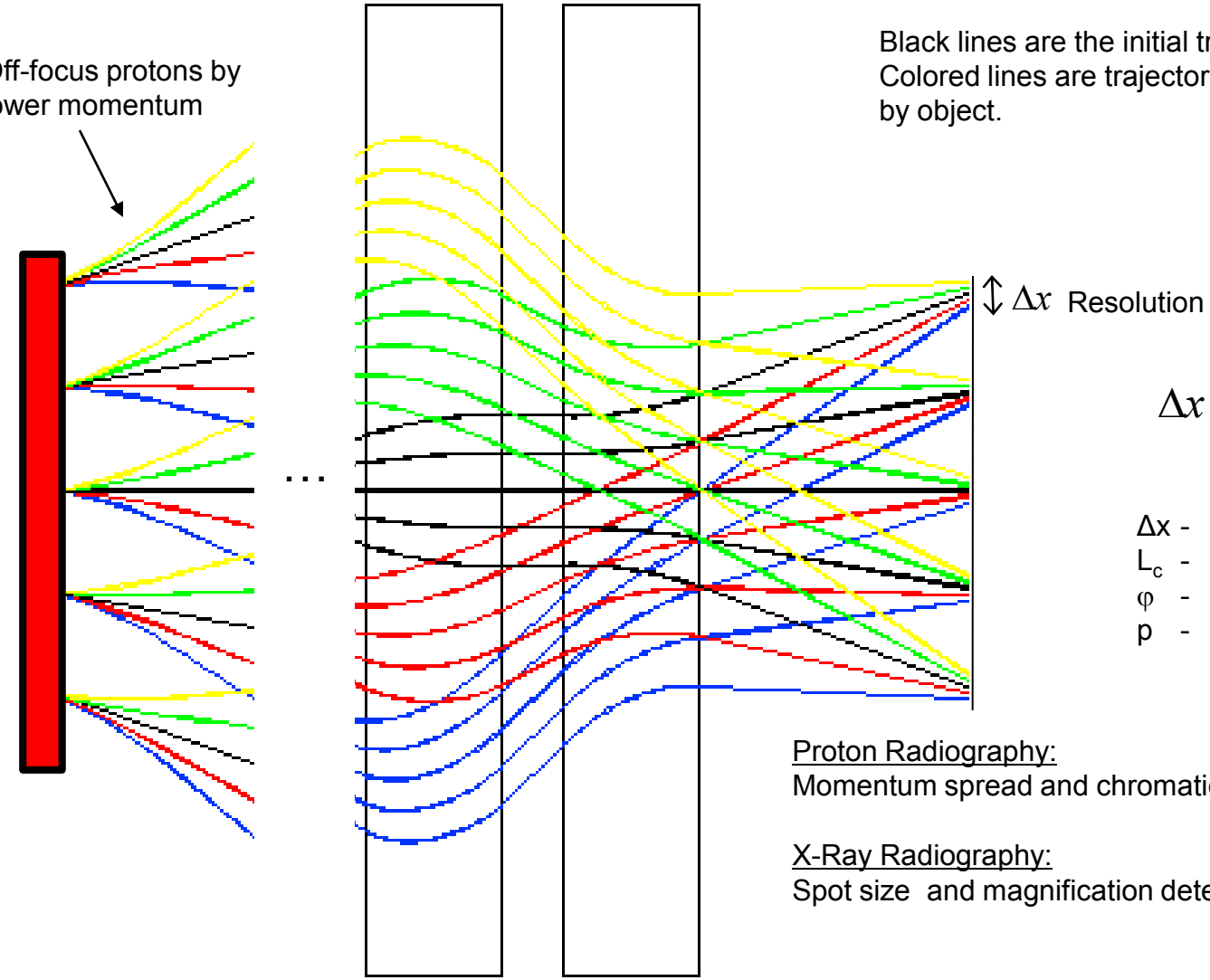

Black lines are the initial trajectories of the protons. Colored lines are trajectories of protons scattered by object.

$$\Delta x = L_c \phi \frac{\Delta p}{p}$$

Δx - Resolution
L_c - Chromatic Length
φ - Scattering angle
p - Momentum

<u>Proton Radiography:</u>
Momentum spread and chromatic length determine the resolution

<u>X-Ray Radiography:</u>
Spot size and magnification determine the resolution.

Chromatic Blur ⟶ Limbing

Limb: To outline in clear sharp detail

Like phase-contrast radiography:

- Useful to enhance edges
- Problem for density reconstruction

Resolution proportional to energy offset

$$\sigma = \theta l_c \frac{E - E_f}{E_f}$$

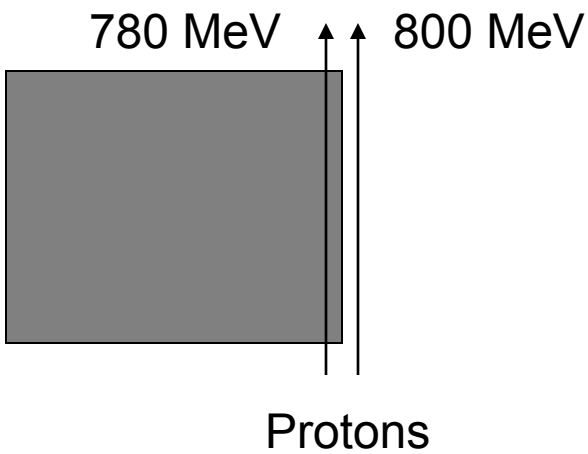

Focus on high energy protons

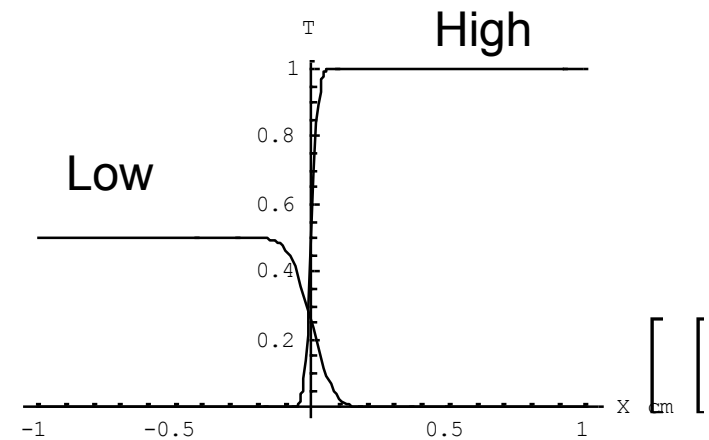

Low + High

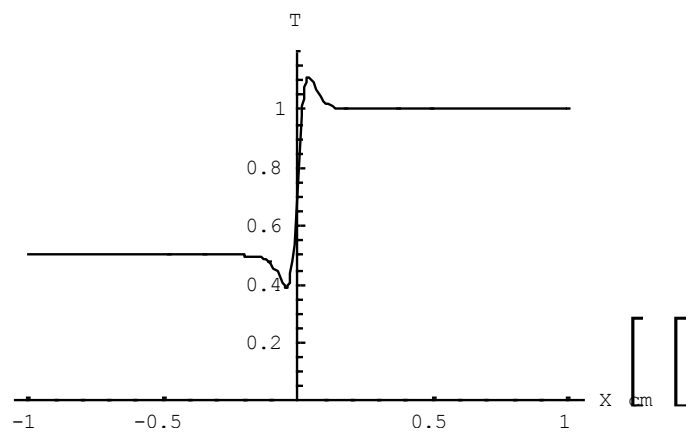

Example: Focused on high energy protons

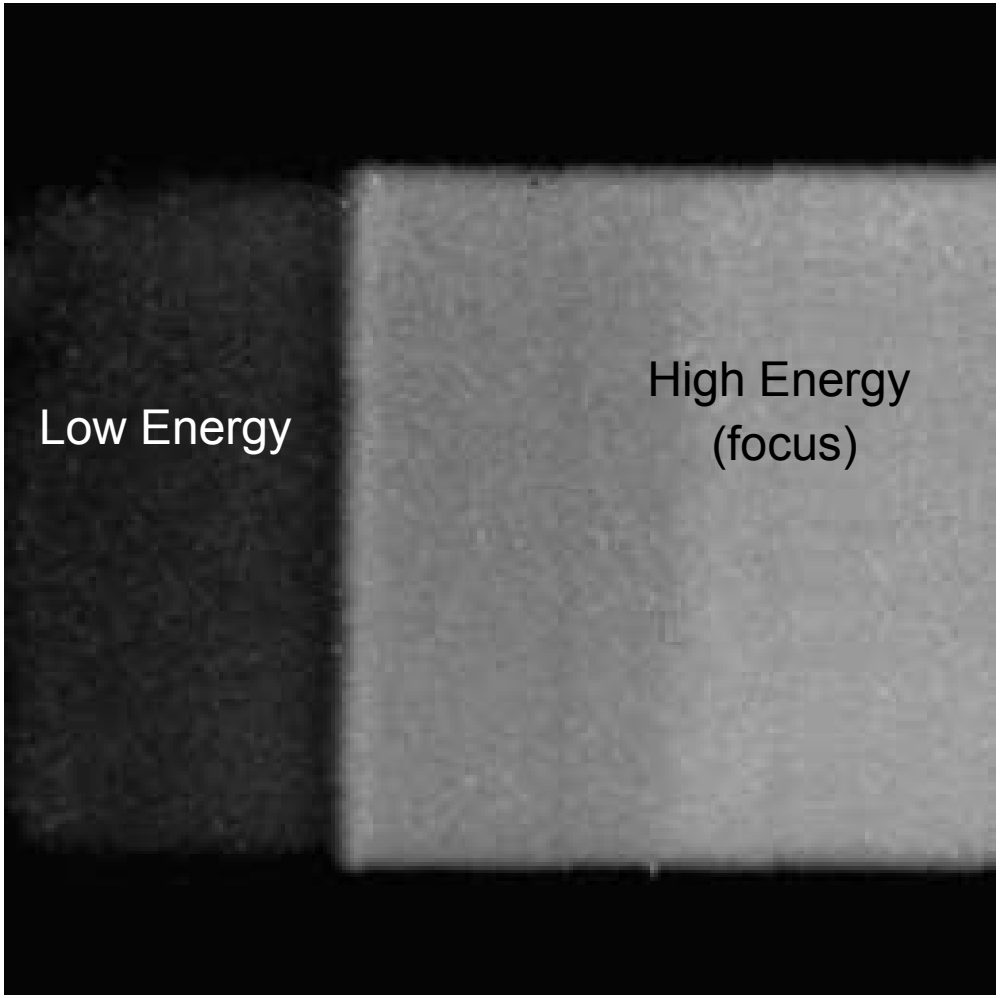

Focus on high energy protons

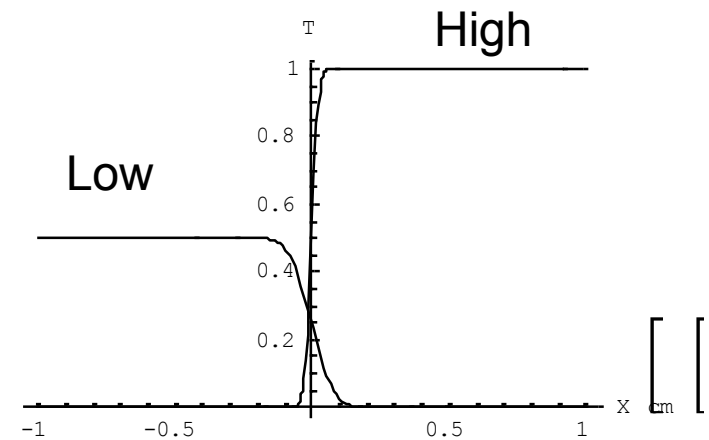

Low + High

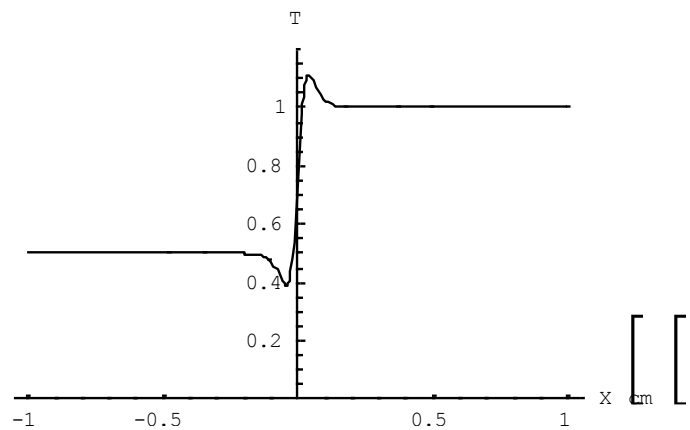

800 MeV x3 Magnifying Imaging Lens

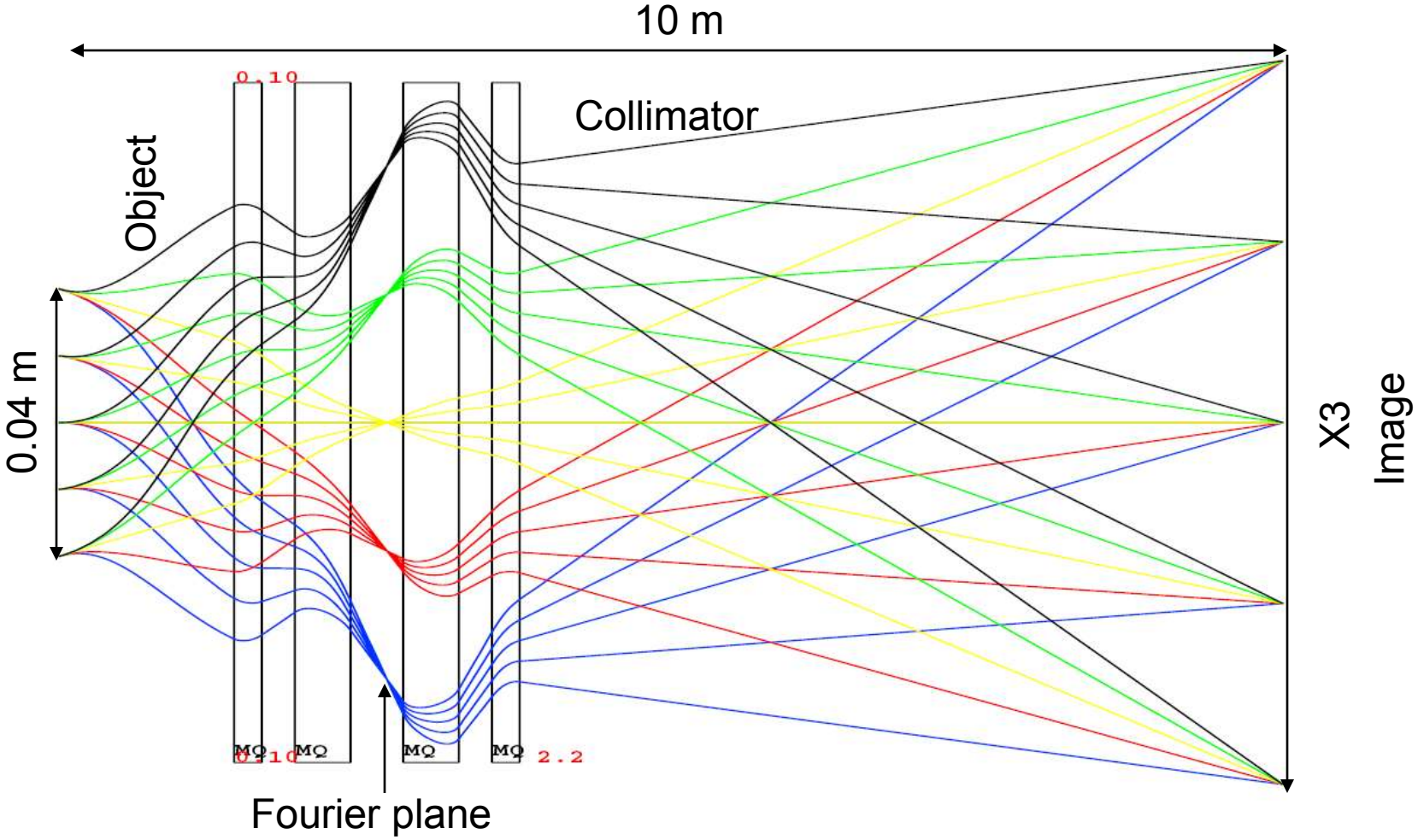

Solid-Solid Phase Transition in Iron

Dramatic Improvement in Resolution is allowing us to make new measurements like this solid-solid phase transition in iron. We are performing experiments with the magnifier to study solid-solid phase transitions in cerium this week.

Identity Lens $\frac{\Delta P}{P} = 8.7\%$

copper

X3 Magnifying Lens $\frac{\Delta P}{P} = 8.1\%$

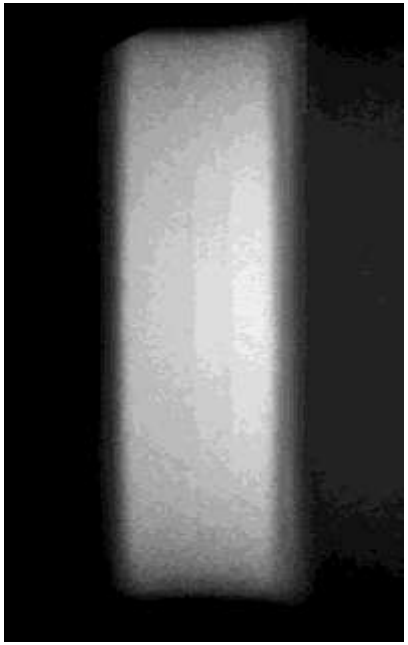

Iron

Resolution improvement equivalent to an energy increase from 800 MeV to 2 GeV (in terms of chromatic blur)

Material Strength Experiments

PTW fit to Hopkinson-Bar data*

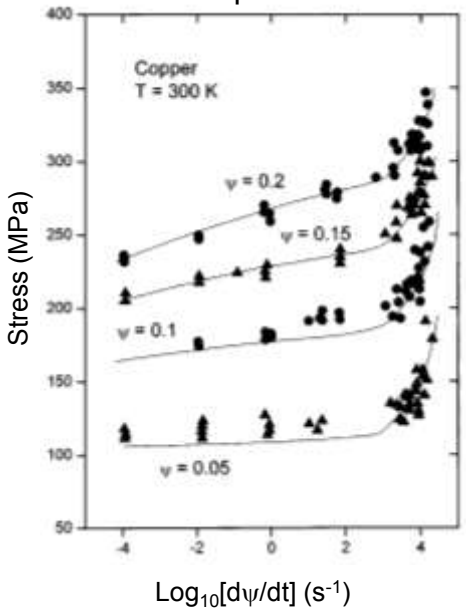

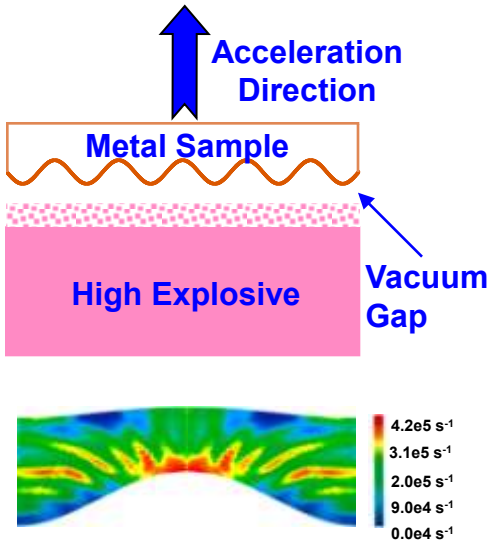

Calculated Strain Rate

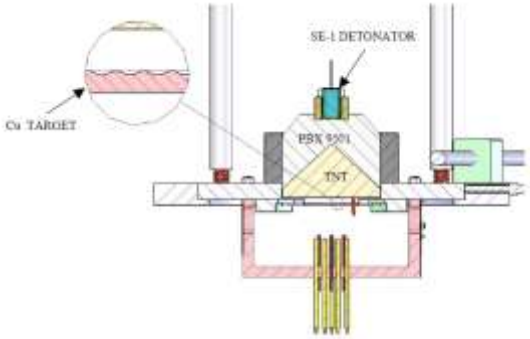

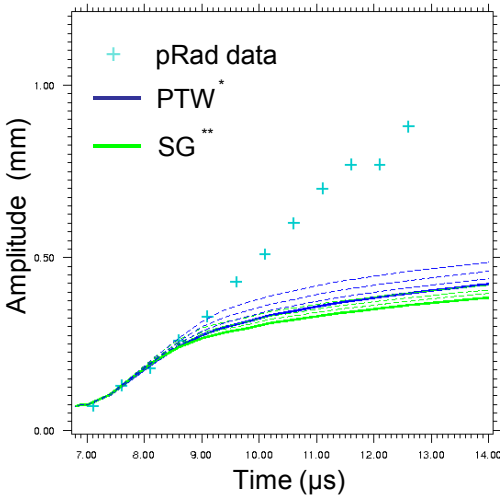

2 mm offset 3 mm offset

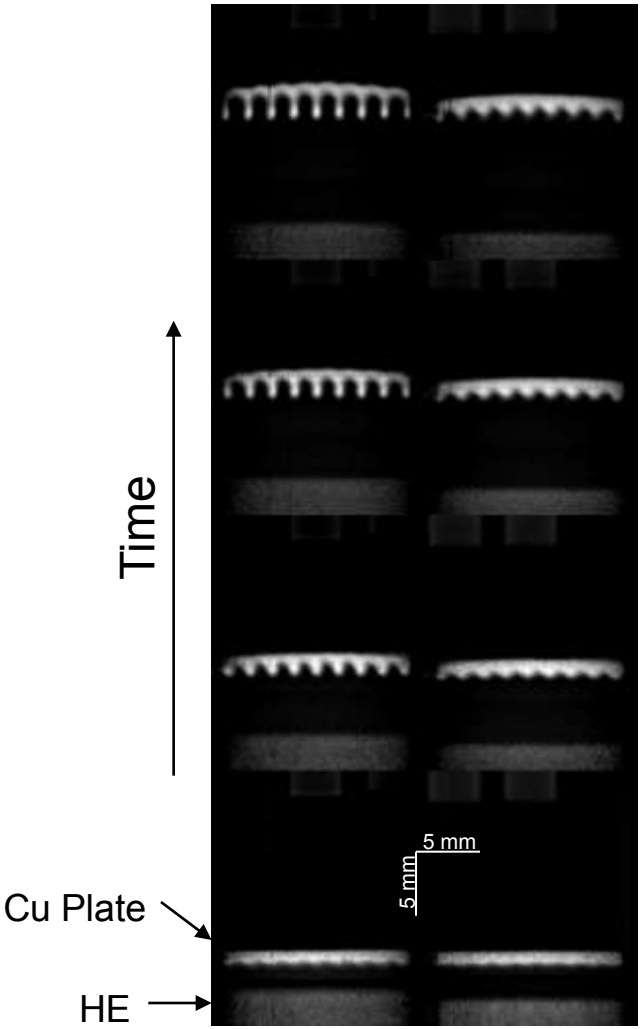

*D.L.Preston, et al. J.Appl. Phys. **93**, 211 (2003).

LA-UR 08-07298

** D. J. Steinberg, et al. J.Appl. Phys. **61**, 1816 (1987).

Material Strength Experiments

PTW fit to Hopkinson-Bar data*

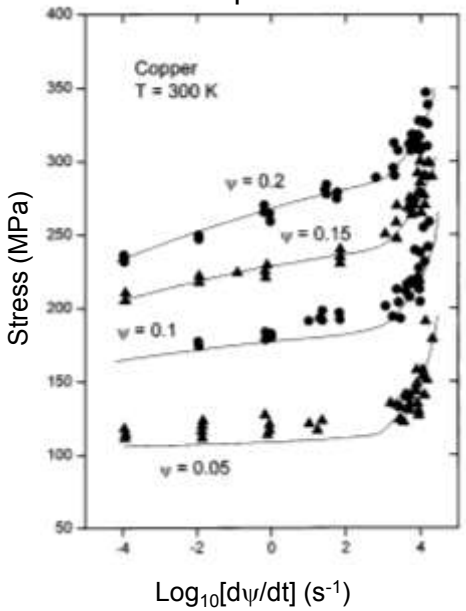

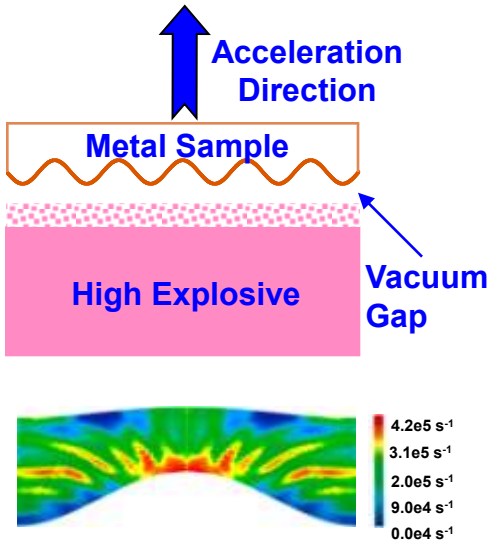

Calculated Strain Rate

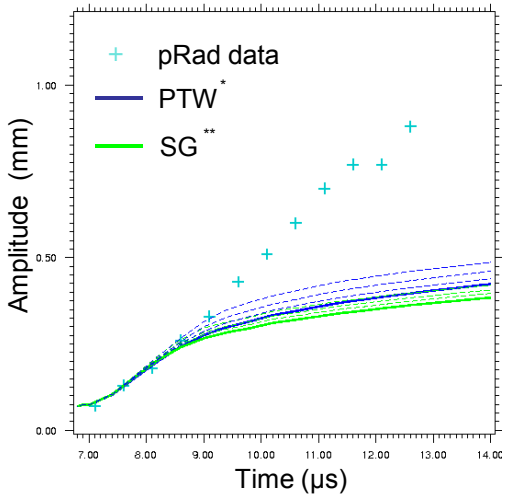

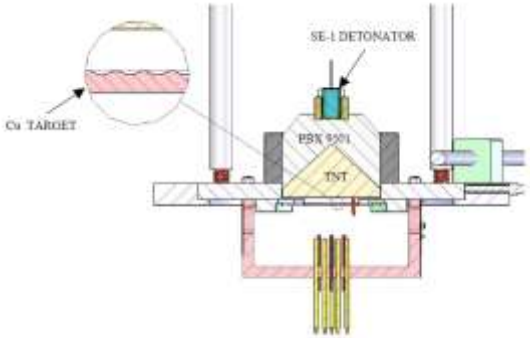

35 μm 55 μm

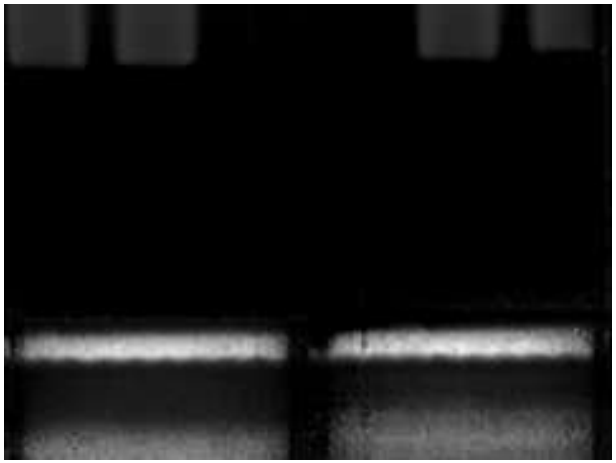

*D.L.Preston, et al. J.Appl. Phys. **93**, 211 (2003).

** D. J. Steinberg, et al. J.Appl. Phys. **61**, 1816 (1987).

Powder Gun Driven Equation Of State Measurements

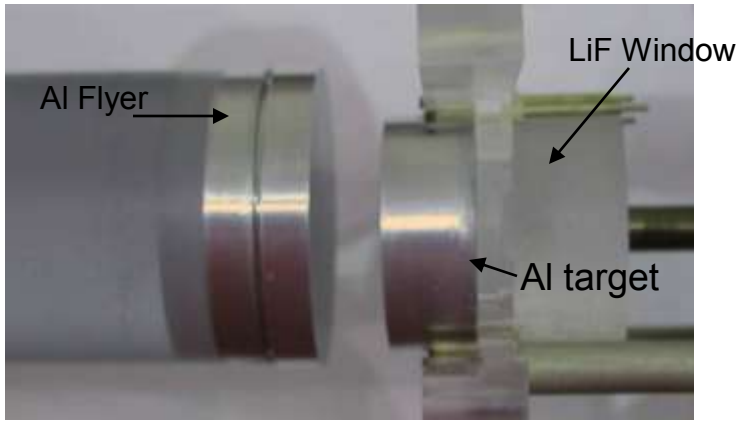

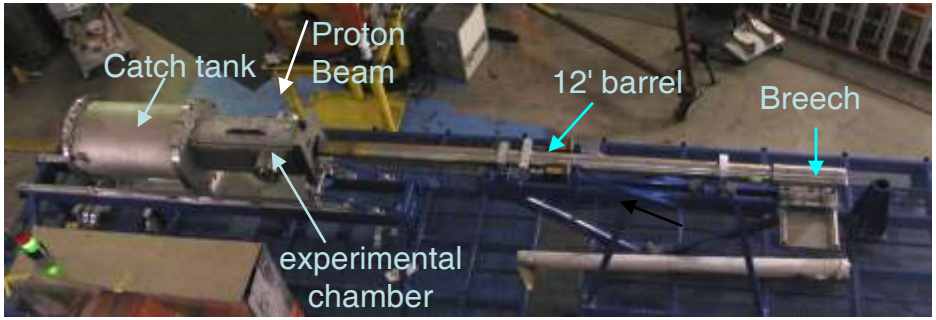

Aluminum

1.4 km/s

Copper

1.4 km/s

Powder Gun Al/Cu Equation Of State

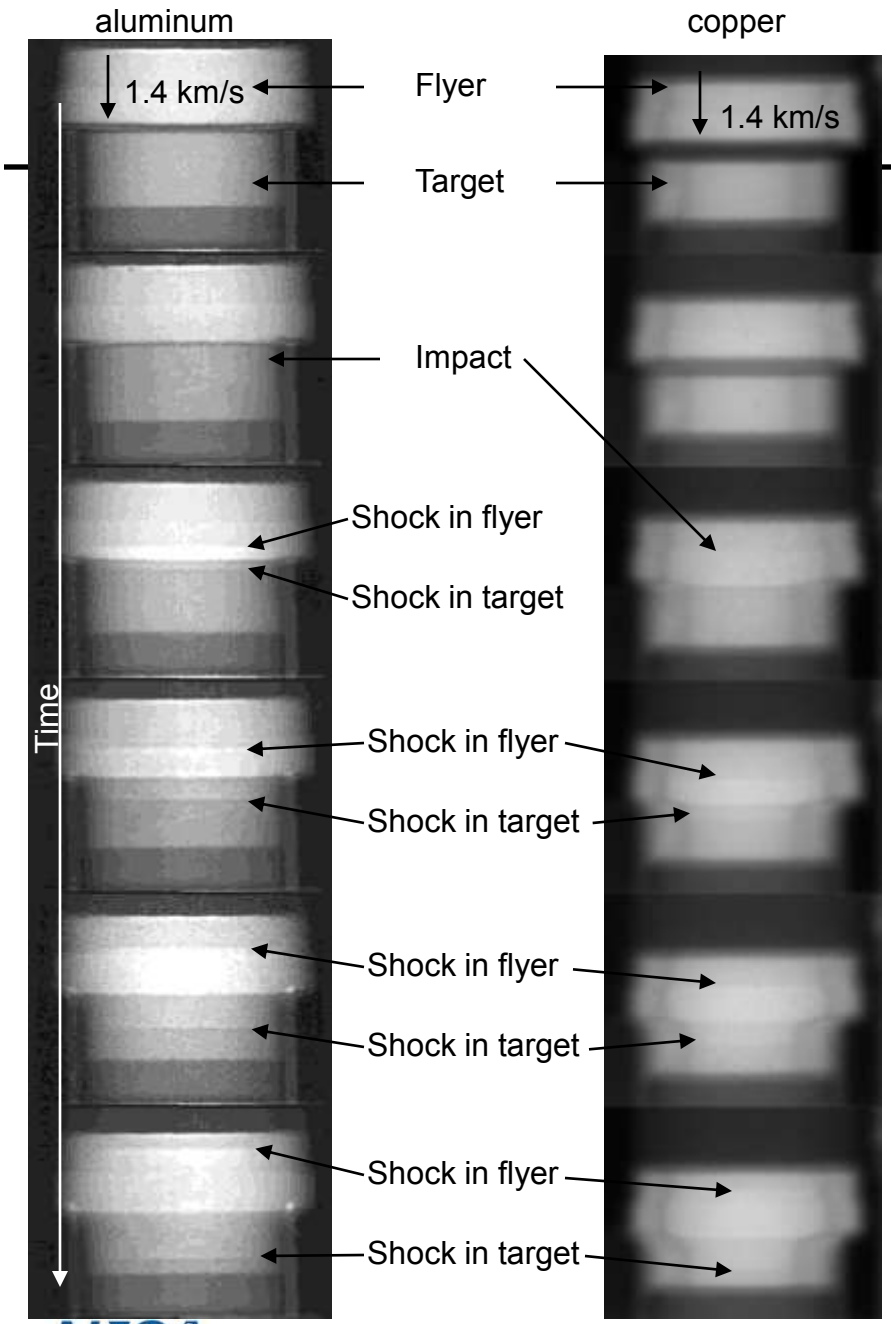

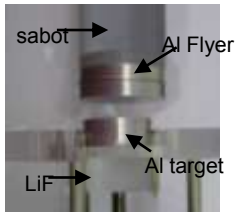

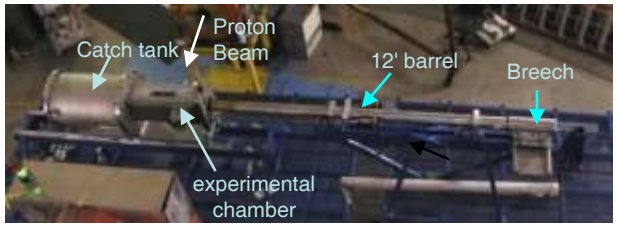

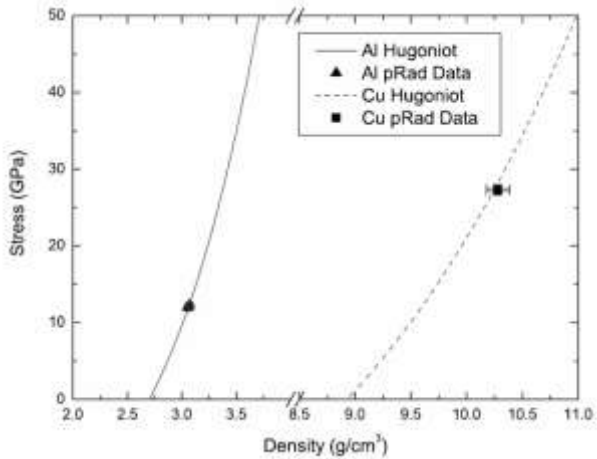

TABLE I. Summary of the experiments with the uncertainties for each quantity shown in parentheses.

Experiment	Impactor/ sample	Impactor velocity (mm/μs)	Peak stress (GPa)	Initial density (g/cm³)	Calculated density (g/cm³)	Measured density (g/cm³)	Agreement
1	Al 6061-T6	1.452 (0.012)	12.27 (0.11)	2.710 (0.003)	3.067 (0.005)	3.070 (0.025)	0.1%
2	Al 6061-T6	1.422 (0.002)	11.98 (0.03)	2.710 (0.003)	3.060 (0.004)	3.056 (0.020)	0.1%
3	OFHC Cu	1.30 (0.04)	28.59 (0.91)	8.928 (0.003)	10.30 (0.05)	10.28 (0.08)	0.2%
4	OFHC Cu	1.249 (0.002)	27.16 (0.06)	8.928 (0.003)	10.241 (0.006)	10.28 (0.08)	0.4%

Solid-Solid Phase Transitions in Iron

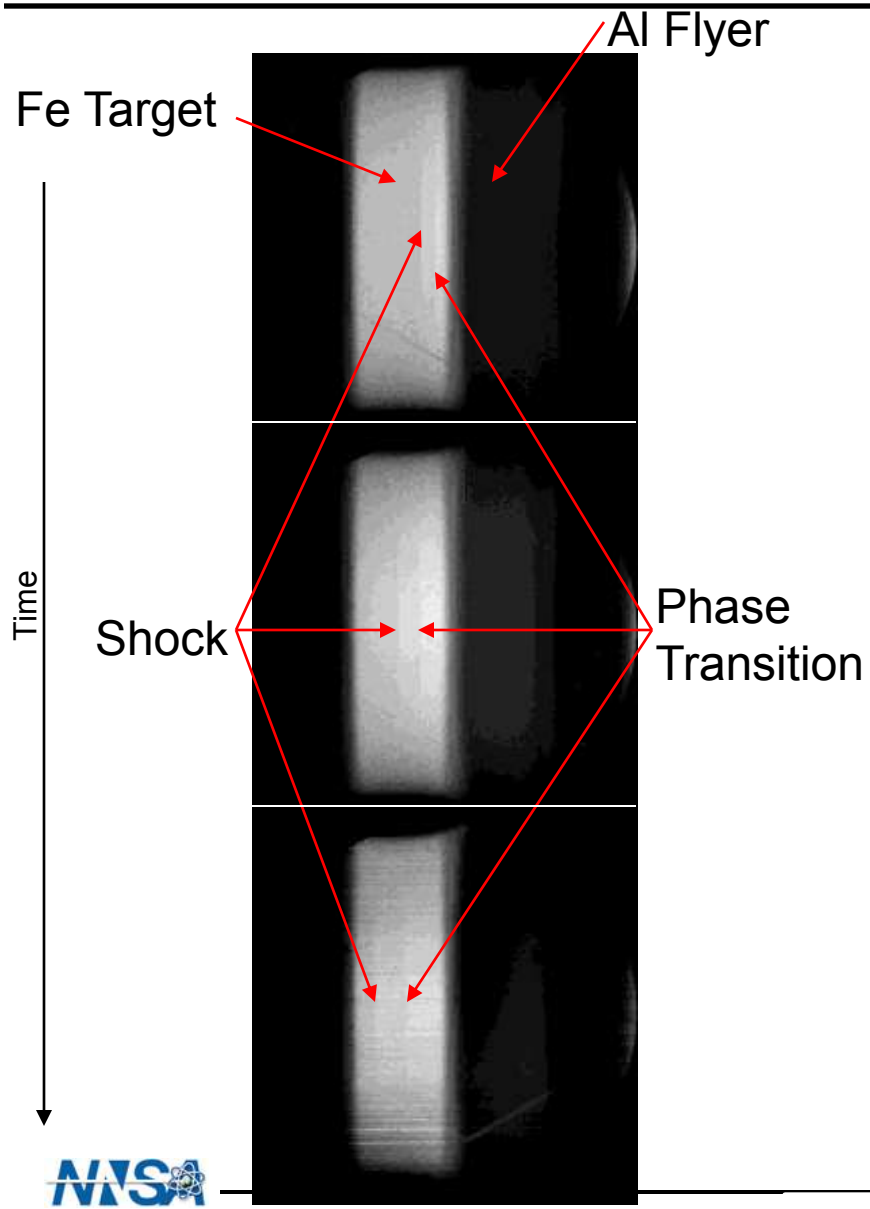

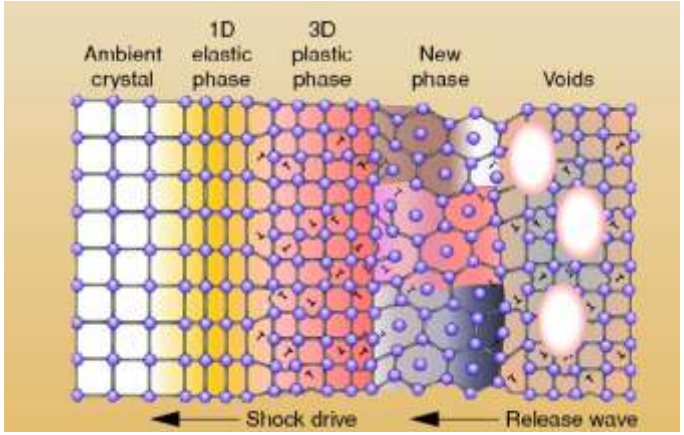

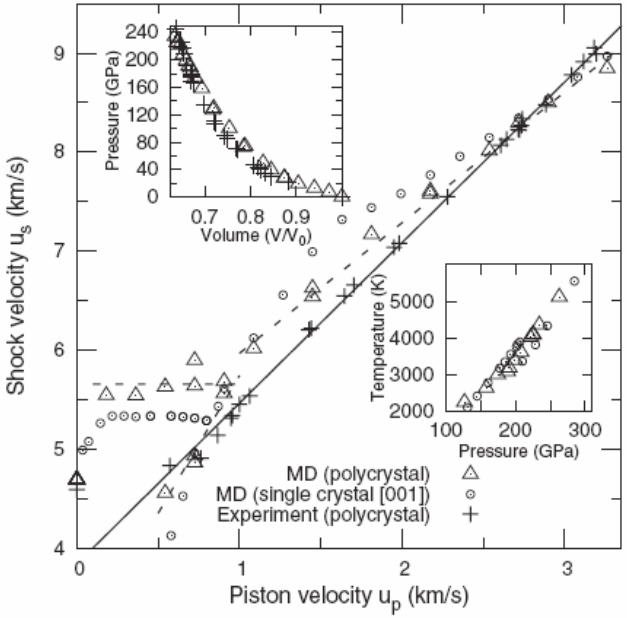

Phys. Rev. Lett. 98 135701 (2007)

pRad has been used to study the failure of materials driven by point detonated high explosives

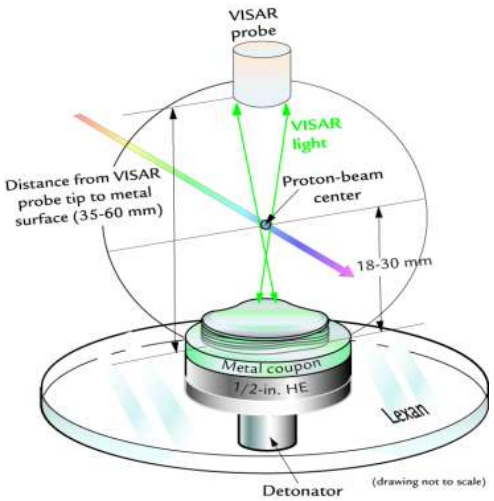

A comparison of spall for different materials

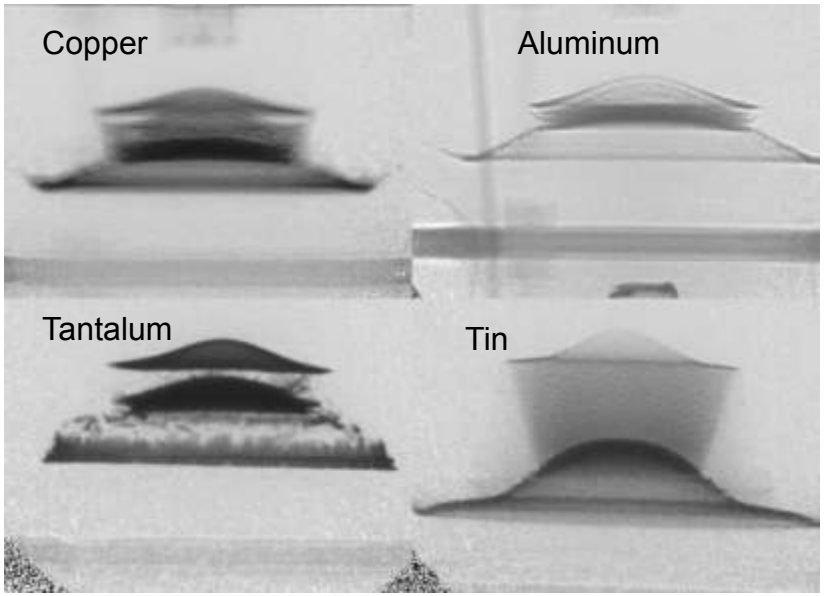

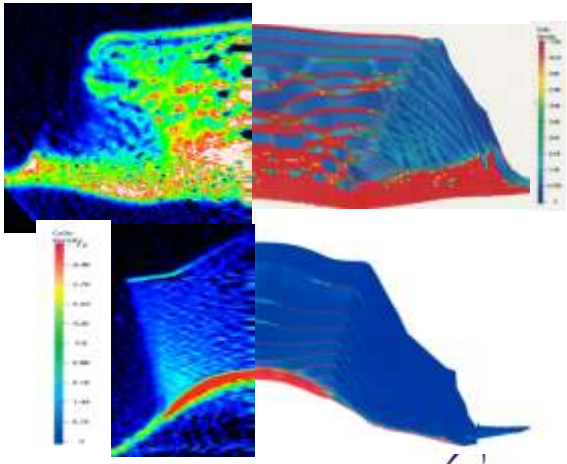

- Experiments were aimed at extending VISAR measurements below the leading spall layer.
- Proton radiographs reveal that the deepest damage layers are not well defined.
- Multiple pRad experiments show that damage formation deep within the metal is “statistical” in nature and dependent on metal.

Complicated Studies of HE Burn Products

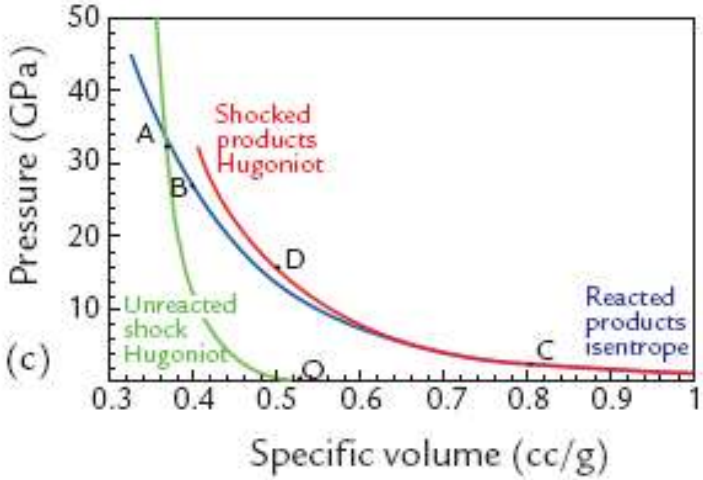

Studies of HE Burn Products

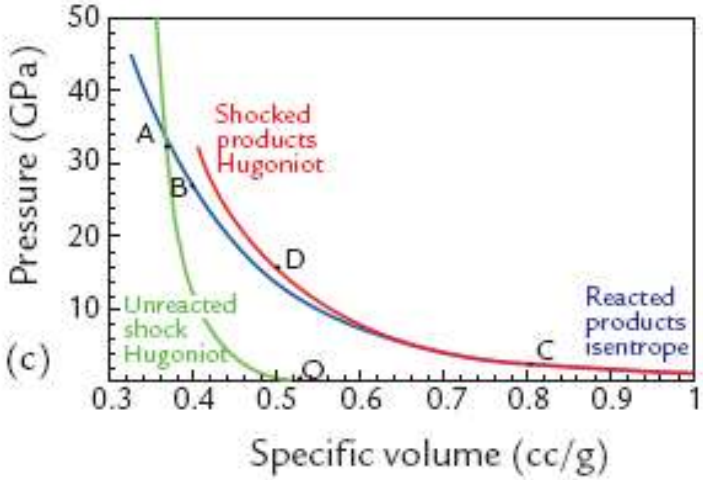

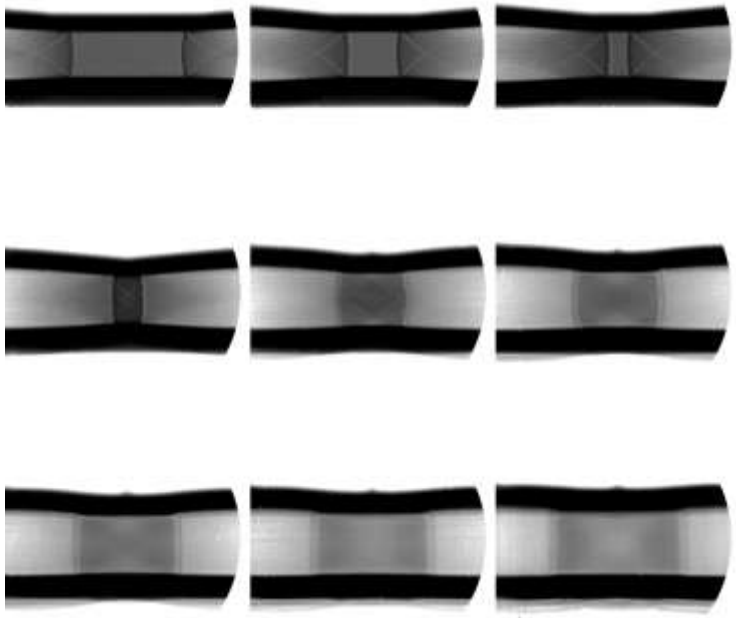

Evolution of Spall Damage

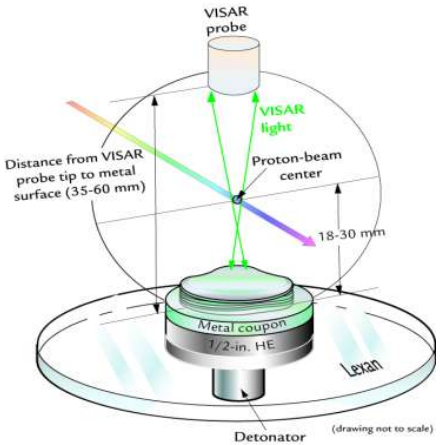

What damage occurs behind the first spall layer?

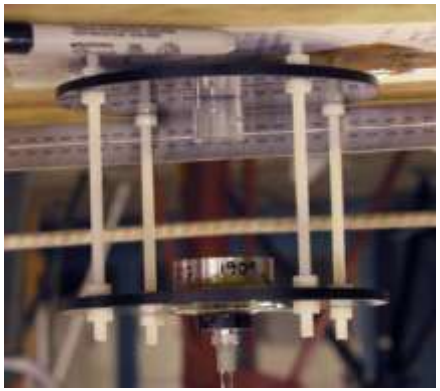

Incipient Spall with Recovery Experiments

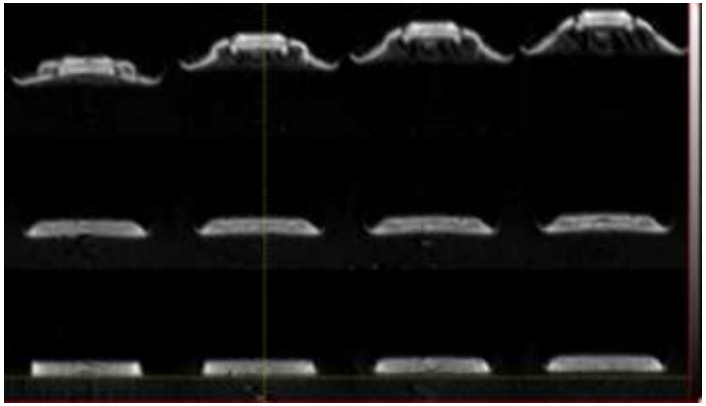

Dynamic Radiograph

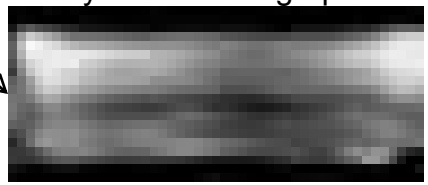

Micrograph

0.8 cm

- How and where are voids formed?
- How do they coalesce to form macroscopic damage?
- Requires improvements in resolution.

Few Hertz Radiographic Movies

- <5 Hz Frame Rate
- 1000 Frame limit

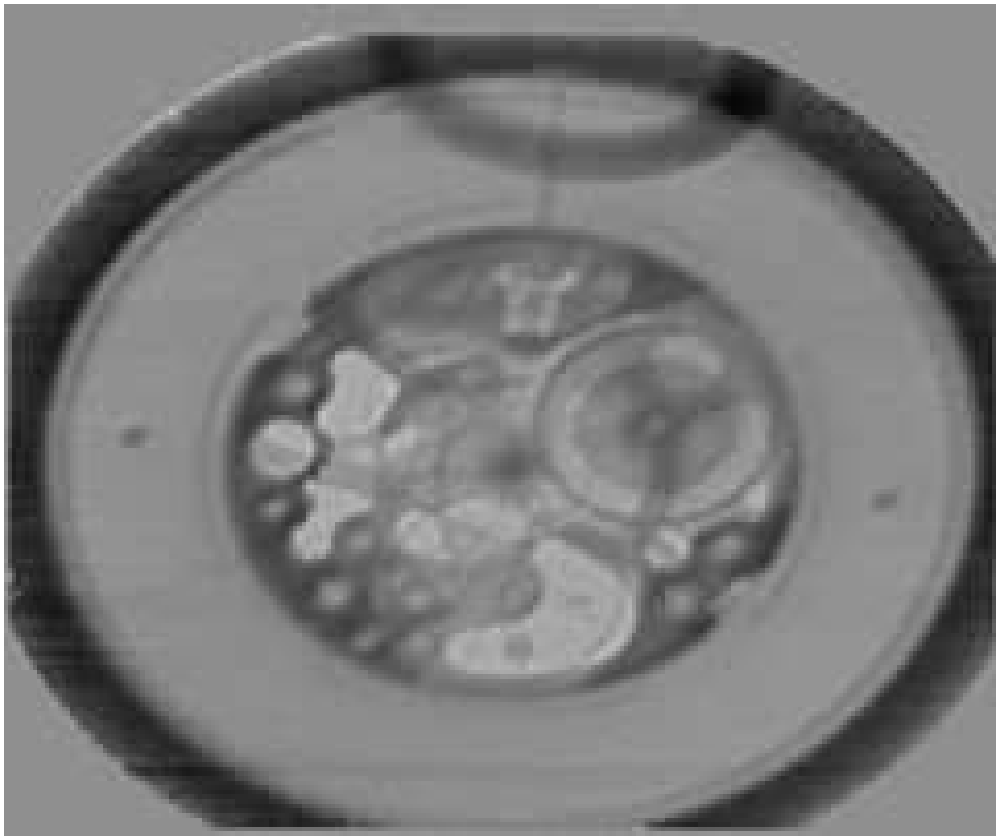

Summary

- 800 MeV proton radiography continues to provide high quality dynamic materials studies for LANL.
- Gains in resolution have been realized through the development of magnifying lens systems.
- Interest at Los Alamos to build a user community for access to 800 MeV proton radiography.
- We will be looking for user experiments in the 2008 run cycle (June-December).